High-spin states in ^{107}Pd, ^{108}Pd, and ^{109}Ag

K. R. Pohl,* P. H. Regan,† J. E. Bush, P. E. Raines, and D. P. Balamuth
Department of Physics, University of Pennsylvania, 209 South 33rd St, Philadelphia, Pennsylvania 19104

D. Ward, A. Galindo-Uribarri, and V. P. Janzen
AECL, Chalk River Laboratories, Chalk River, Ontario, Canada K0J 1J0

S. M. Mullins
Department of Physics and Astronomy, McMaster University, Hamilton, Ontario, Canada L8S 4M1

S. Pilotte‡
Department of Physics, University of Ottawa, Ottawa, Ontario, Canada K1N 6N5
(Received 14 November 1995)

High-spin states in ^{107,108}Pd and ^{109}Ag have been studied by charged-particle-γ, γ-γ, and charged-particle-γ-γ coincidence measurements of heavy-ion fusion-evaporation reactions. The high-spin level schemes of these nuclides have been significantly extended and new deformed rotational bands have been found in each nuclide. These bands exhibit the general property of back bends corresponding to the rotational alignment of a pair of $h_{11/2}$ quasineutrons. Band properties are compared with predictions of the cranked shell model and total Routhian surface calculations. The properties of the yrast and near-yrast bands of all three nuclides are generally consistent with predictions of moderate ($\beta_2 \approx 0.2$) prolate deformation. [S0556-2813(96)00806-0]

PACS number(s): 21.10.Re, 23.20.En, 23.20.Lv, 27.60.+j

I. INTRODUCTION

The interaction between the $Z=50$ spherical shell gap and the deformation-driving effects of the $h_{11/2}$ neutron intruder orbital results in a variety of collective behavior in the stable and neutron-rich nuclei below the shell gap. For instance, a number of prolate-deformed rotational bands have recently been reported in $^{105-111}$Cd [1–8], nuclides whose low-energy collective states are well described as vibrational excitations. Similar prolate-deformed rotations have been found in $^{104-107}$Ag [9–11] and $^{103-106}$Pd [12–14], with superdeformed bands reported in $^{103-105}$Pd [12,14]. At larger neutron numbers, oblate-deformed rotations have recently been reported in ^{112,114,116}Pd [15], as have triaxial rotations in ^{108,110,112,114}Ru [16]. However, the bulk of this work has concentrated on nuclei away from the region where shape transitions have been predicted by interacting boson approximation (IBA) (cf. [15]) and microscopic Hartree-Fock-Bogoliubov (HFB) calculations [17]. In the present work, we have studied high-spin states in the intermediate nuclides ^{109}Ag and ^{107,108}Pd with the aim of extending our knowledge of nuclides in this region and investigating possible shape-transitional effects.

Two experimental techniques have been applied to study high-spin states in nuclides in this region, both of which rely on large Ge detector arrays to gather γ-γ coincidence data. Heavy-ion fusion-evaporation reactions have been used to populate light Cd, Ag, and Pd nuclides. Unfortunately, the lack of appropriate beam-target combinations and the small cross sections for charged-particle evaporation channels have largely prevented the use of these reactions for heavier systems. Alternately, spontaneous fission sources can be used to populate Ru and heavy ($A>110$) Pd nuclides, but are less useful for lighter isotopes. Although some of the nuclides in the middle of this region are stable (including ^{109}Ag and ^{108}Pd) little is known about their high-spin excited states. To bridge the gap between the two measurement methods, we have used a high-efficiency charged-particle array in conjunction with Ge detectors to enhance the low-yield pxn and αxn evaporation channels through which these nuclides can be populated in heavy-ion fusion reactions.

II. EXPERIMENTAL PROCEDURE AND ANALYSIS METHODS

Experiments were carried out at both the University of Pennsylvania tandem Van de Graaff accelerator and the Tandem Accelerator Super-Conducting Cyclotron (TASCC) Facility of AECL at the Chalk River Laboratories. At both facilities, the nuclides of interest were populated via fusion-evaporation reactions with an ^{18}O beam incident on thin ^{96}Zr targets (1 mg/cm^2 at Penn, 600 μg/cm^2 at Chalk River). In both cases, the targets were enriched to 85% ^{96}Zr, with ^{90}Zr comprising the bulk of the remainder. An additional experiment was performed at the University of Pennsylvania using a ^{13}C beam and a ^{100}Mo target enriched to greater than 99% ^{100}Mo.

In the ^{18}O+^{96}Zr experiment performed at the University

*Present address: National Air and Radiation Environmental Laboratory, 540 S. Morris Ave., Montgomery, Alabama 36115-2601.

†Present address: Department of Physics, University of Surrey, Guildford, Surrey, GU2 5XH, United Kingdom.

‡Present address: Centre de Recherches Nucléaire, Institut National de Physique Nucléaire et de Physique des Particules/ Université Louis Pasteur, F-67037 Strasbourg Cedex, France.

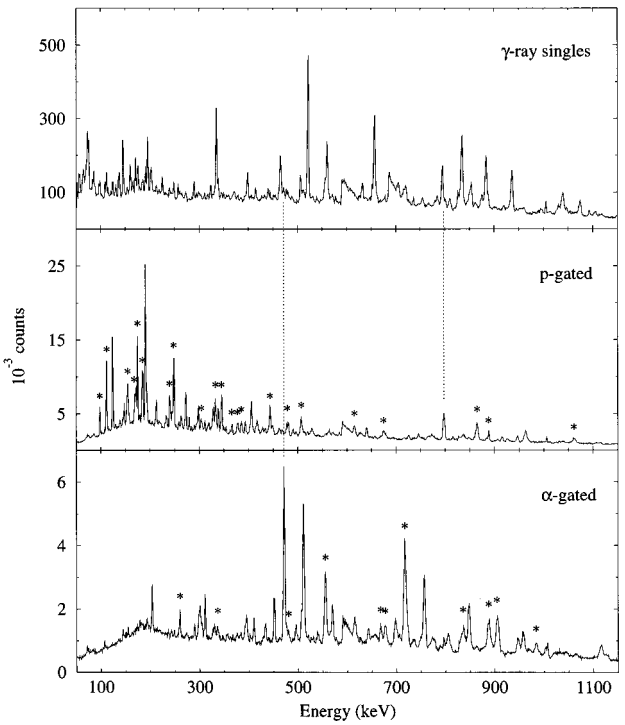

FIG. 1. Singles, proton-gated, and α-gated γ-ray spectra from the University of Pennsylvania ^{18}O+^{96}Zr experiment at $E_{\text{beam}}=72$ MeV. The singles spectrum has been multiplied by 100 to compensate for a hardware downscale. The dotted lines indicate the strongest pxn and αxn γ rays, which are obscured in the singles spectrum by γ rays from xn channel products. Asterisks in the coincidence spectra mark peaks partially or wholly due to reactions on $^{90-94}$Zr.

of Pennsylvania, γ rays were detected in two Compton-suppressed, 25% relative efficiency germanium detectors located at angles of 45° and 90° with respect to the beam axis. Thirteen elements of the Penn 4π array [18] (a segmented phoswich charged-particle detector array) subtending about 60% of 4π sr, were used to select proton and α-particle evaporation channels. Data were recorded for events in which a suppressed γ ray was detected in coincidence with a charged particle, and for a fraction of γ-ray singles events. Intensities, angular distributions, and excitation functions for γ rays in coincidence with protons and α particles were measured for beam energies of 56, 63, 72, and 80 MeV. Approximately 20 million particle-γ coincidences were recorded at each energy. Additional measurements were made using a 1 mg/cm^2 $^{\text{nat}}$Zr target in order to assess the level of contamination due to reactions with the light Zr isotopes. As with the other experiments described here, γ-ray efficiencies and energy calibrations were determined using ^{152}Eu and ^{133}Ba sources placed at the target position.

The bulk of fusion events (>90%) from the ^{18}O+^{96}Zr reaction proceed via neutron evaporation to $^{109-111}$Cd. Given the fact that few, if any, high-spin states were previously known in the nuclides of interest, the usefulness of a high-efficiency charged particle detector in selecting the very weak proton- and α-evaporation channels is clear. This is illustrated in Fig. 1, where proton- and α-gated spectra at $E_{\text{beam}}=72$ MeV are compared to an ungated spectrum. The strongest charged-particle coincident γ rays (the 473 keV γ-ray in ^{107}Pd and a previously unknown 798 keV γ-ray in ^{109}Ag) are indicated with dotted lines. Note that both are dwarfed by neighboring Cd lines (the 796 keV $8^+\rightarrow 6^+$ in ^{110}Cd and the 466 keV $25/2^-\rightarrow 21/2^-$ in ^{109}Cd.)

The results of this experiment were used primarily to identify optimal beam energies for producing the nuclides of interest, for initial identification of γ rays in Ag isotopes, and for determining the magnitude of the contamination of the charged-particle coincidence spectra due to reactions on light zirconium isotopes. Note that although the target was enriched to 85% ^{96}Zr, the cross sections for charged-particle emission from reactions on ^{96}Zr were much smaller than those for reaction on $^{90-94}$Zr, so that nearly half of all events with emitted protons or α particles came from the lighter isotopes. Some of the peaks in the particle-coincident γ-ray spectra in Fig. 1 which are partially or wholly due to reactions on light zirconium isotopes are indicated with asterisks. Clearly, interference from these contaminant transitions (especially in the proton-coincident spectrum) greatly increases the difficulty of obtaining useful spectroscopic information on these nuclides from particle-γ coincidence data.

While the interference from the overwhelming xn evaporation channels is most easily removed by using a charged-particle coincidence technique, the interference due to the light Zr isotopes is best overcome with γ-γ coincidence methods. An excellent combination of the two is provided by the 8π and ALF detector arrays at the TASCC facility of the Chalk River Labs. We measured γ-γ coincidences with the 8π spectrometer [19], which consists of 20 Compton-suppressed Ge detectors (each 25% relative efficiency) arranged in four rings of five detectors each. Two rings lie 37° off the beam axis at forward and backward angles, while the other two lie 79° off the beam axis. A 70-element bismuth germanate (BGO) inner ball provided the total γ-ray fold (K) and sum energy (H) for each event. Coincident charged particles were detected and identified with an array of 24 CsI(Tl) detectors [20], which covered about 85% of 4π sr. Data were recorded for events in which at least two suppressed γ rays were detected in the 8π array in prompt coincidence with at least five segments of the BGO ball. Approximately 150 million events were recorded at $E_{\text{beam}}=70$ MeV. Of these, protons were identified in about three million events and α particles were identified in about two million. Approximately 50 million events were recorded at 60 MeV, with proton and α coincidences forming less than 0.5 million events, each.

Data from the Chalk River experiment were sorted off line into separate γ-γ matrices for ^{107}Pd, ^{108}Pd, and ^{109}Ag analysis (after unfolding higher Ge-detector multiplicities.) For each matrix, particle-identification cuts on the CsI(Tl) data and H and K cuts on the BGO ball data were used to emphasize the channel of interest. Analyses were also performed on the γ-γ data from $5n$- and $3n$ evaporation leading to ^{109,111}Cd. The results of these analyses have already been published [6].

Transition intensities were determined from fits to the total projection spectrum of each matrix when possible, or from selected coincidence spectra. Information about γ-ray multipolarity was determined using a gated angular distribution method. In this method, two γ-ray energy matrices (labeled ''37° matrix'' and ''79° matrix'') are generated. If the

first γ ray of a γ-γ pair is detected at 37° (or 143°), the (E_1,E_2) element of the 37° matrix is incremented, regardless of where the second γ ray is detected. (E_1 and E_2 refer to the energies of the first and second γ rays, respectively.) Similarly, if the first γ ray is detected at 79° (or 101°), the (E_1,E_2) element of the 79° matrix is incremented. The process is then repeated, with the detection angle for the second γ ray determining in which matrix the (E_2,E_1) element is incremented. For a given γ-γ pair, either the 37° matrix is incremented twice, or the 79° matrix is incremented twice, or each is incremented once. The angular distribution of a γ ray can be determined by placing gates on coincident lines, projecting both matrices onto the x axis, and comparing the intensities of the peak of interest.

We define an anisotropy

$$A = 2\left(\frac{I_{37°} - I_{79°}}{I_{37°} + I_{79°}}\right) \tag{1}$$

where $I_{37°}$ is the intensity in the 37° matrix projection, and $I_{79°}$ is the intensity in the 79° matrix projection. For initial states with fully aligned magnetic substate distributions, stretched quadrupoles will have $A > 0.4$, and stretched dipoles will have $A < -0.2$. Generally, the initial state will not be fully aligned and the anisotropy will be attenuated by a factor α: $A = \alpha A_0$, where A_0 is the fully aligned anisotropy. In principle, the attenuation for a particular state depends on the details of the reaction used and the spins of the feeding states. In practice, α can be taken to be a monotonically increasing function of excitation energy, with values from known transitions used as guides. Typical anisotropies in this experiment were $A \approx 0.3$ for $\Delta I = -2$ quadrupoles, $A \approx -0.3$ for $\Delta I = -1$ dipoles, and $-1 < A < 1$ for mixed $\Delta I = -1$ transitions. Figure 2 shows calculated anisotropies for various pure and mixed transitions.

The principal advantage of the gated angular distribution technique over the more common directional correlation of orientation (DCO) technique is that the multipolarity of the gating transition need not be known since correlations between the two γ rays are ''averaged out'' by gating at both angles. This is especially useful for analyses of weak, mixed $\Delta I = -1$ bands. Disadvantages include the need to determine the substate alignment α, and the requirement of many detectors at each angle in order to remove correlations. (The method obviously fails for fewer than two detectors at each angle, and errors of order 0.05 can exist even for the 8π array, which has ten detectors at each angle. Note, however, that these errors can be reduced by combining results from different gates.)

Since the reactions used preferentially populate near-yrast states, we discount transitions which increase the nuclear spin. Consequently, transitions with $A \leq -0.05$ can be assigned as $\Delta I = -1$. Positive anisotropies can result from $I \rightarrow I$, $I \rightarrow I-2$, or mixed $I \rightarrow I-1$ decays. However, $\Delta I = 0$ transitions are usually accompanied by competing $\Delta I = -1$ or -2 decays, and we take the absence of such as evidence against a $\Delta I = 0$ assignment. Considerations such as the overall decay pattern and the plausible size of $E2$ matrix elements were also used to choose among the possible multipolarities and mixing ratios.

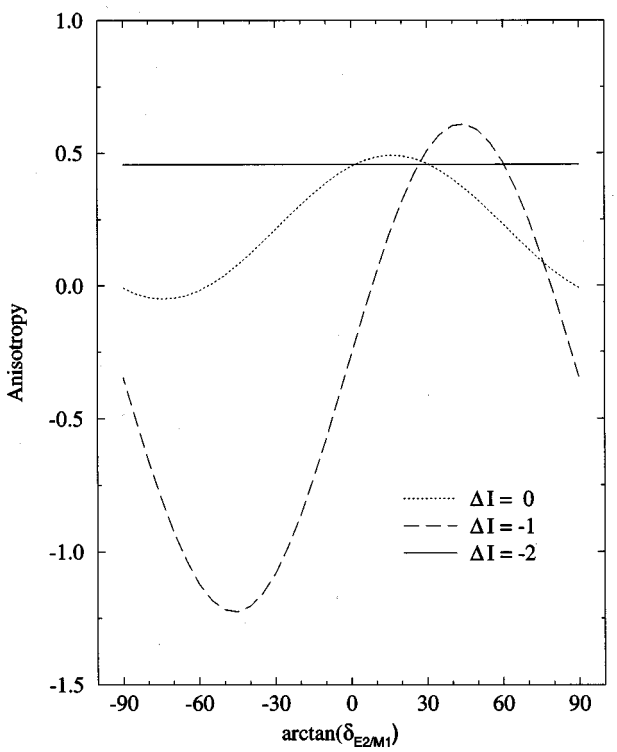

FIG. 2. Calculated fully aligned anisotropies of mixed $E2/M1$ decays. Initial and final state spins are $10 \rightarrow 10$ (dotted), $10 \rightarrow 9$ (dashed), and $10 \rightarrow 8$ (solid; pure $E2$). Anisotropies are reasonably insensitive to spin for initial state spins greater than $4\hbar$. The sign convention for $\delta_{E2/M1}$ is that of Ref. [28].

An experiment designed to detect very-low-energy γ rays ($E_\gamma < 200$ keV) was performed at the University of Pennsylvania using a 65 MeV ^{13}C beam incident on a thin (1 mg/cm^2 ^{100}Mo target (>99% enrichment). Events were recorded for prompt or delayed coincidences between a low-energy photon spectrometer (LEPS) and a Compton-suppressed 25% relative efficiency germanium detector, as well as for a fraction of γ-ray singles events in each detector. The detectors were located at angles of $\theta = 90°$ with respect to the beam axis, and the azimuthal angle between the two detectors was 180°. Unlike the other experiments, no charged-particle detectors were used. Approximately 3×10^5 γ-γ events were recorded on tape.

III. EXPERIMENTAL RESULTS AND LEVEL SCHEMES

A. ^{108}Pd

Prior to this work, firm knowledge of the ^{108}Pd yrast level scheme was limited to states with I^π of up to 6^+ in the ground-state band, based on radioactive decay [21], inelastic scattering [22], and Coulomb excitation [23]. Tentative 8^+ and 10^+ states were reported from fission-fragment spectroscopy experiments [24]. Negative-parity states with spins 3, 4, and 5 were known from inelastic scattering, transfer reactions, and Coulomb excitation reactions.

Preliminary results of the present work for ^{107,108}Pd, including level schemes, have already been presented [25]. The partial level scheme of ^{108}Pd produced from analysis of the Chalk River data is shown in Fig. 3. In addition to five transitions previously reported in ^{108}Pd, 14 new γ rays were

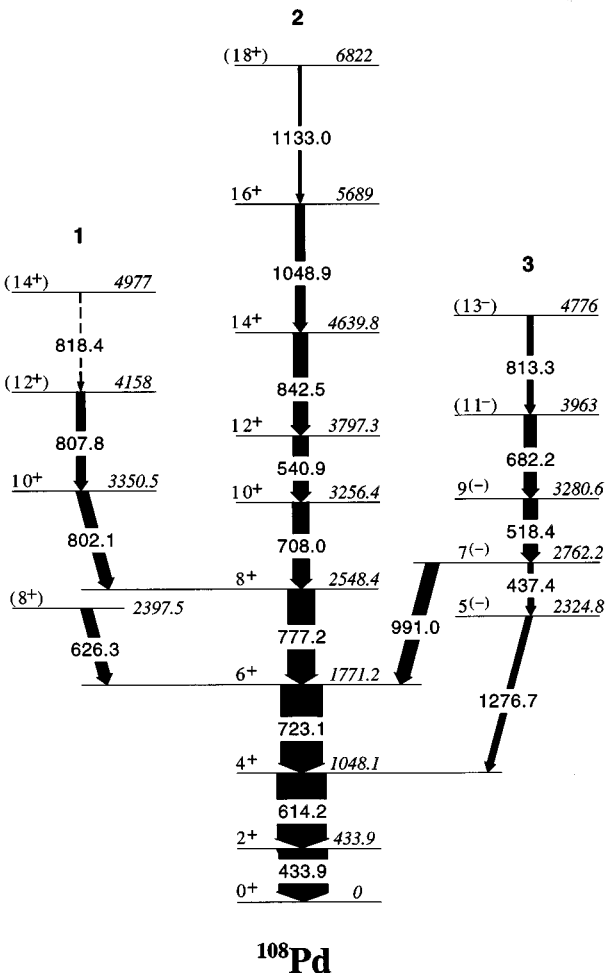

FIG. 3. Level scheme of ^{108}Pd.

identified and placed in the level scheme. The properties of these transitions are tabulated in Table I. The first and second columns of the table give the γ-ray energy and intensity. Due to the small production cross section for ^{108}Pd, listed intensities are taken from a spectrum gated on the 433.9 keV $2^+\rightarrow 0^+$ transition. The measured anisotropy is listed in column 3, and the deduced initial and final state spins are shown in column 4.

The ground band of ^{108}Pd (band 2 in Fig. 3) has been extended through a back bend to 18^+. Figure 4 shows a summed spectrum for the ^{108}Pd ground-state band, produced by gating on the 708.0, 777.2, and 540.9 keV lines. The 2548.4 keV 8^+ state reported by Ref. [24] is seen as a member of this band, but the 3350.5 keV 10^+ state reported in that work is identified as part of a non-yrast sideband (band 1) similar to one seen in ^{110}Cd [8], and may be a continuation of the nonaligned ground-band configuration. This band is seen to a 12^+ state, with a tentative 14^+ state. A definite assignment of this state is precluded by the relative weakness of the depopulating 818.4 keV γ ray, together with interference from an 813.3 keV transition in band 3.

The isotone ^{110}Cd exhibits the unusual feature of three nearly degenerate 8^+ states. Similar, though less pronounced, degeneracies occur in ^{106,108}Cd [3,5] and ^{102,104}Pd [13]. In contrast, a detailed study of ^{106}Pd [13] revealed only one 8^+ state. In the present work, a candidate second

TABLE I. Properties of γ rays placed in ^{108}Pd.

Energy (keV)	Relative intensity	Anisotropy	$I_i^\pi\rightarrow I_f^\pi$
433.9 (1)		0.05 (6)	$2^+\rightarrow 0^+$
437.4 (10)	15 (2)		$7^{(-)}\rightarrow 5^{(-)}$
518.4 (2)	29 (3)	0.13 (22)	$9^{(-)}\rightarrow 7^{(-)}$
540.9 (1)	31 (3)	0.12 (13)	$12^+\rightarrow 10^+$
614.2 (1)	100 (5)	0.12 (7)	$4^+\rightarrow 2^+$
626.3 (4)	23 (3)	0.61 (33)	$(8^+)\rightarrow 6^+$
682.2 (6)	25 (3)	0.09 (24)	$(11^-)\rightarrow 9^{(-)}$
708.0 (1)	34 (4)	0.27 (13)	$10^+\rightarrow 8^+$
723.1 (1)	85 (5)	0.24 (9)	$6^+\rightarrow 4^+$
777.2 (1)	55 (4)	0.17 (10)	$8^+\rightarrow 6^+$
802.1 (3)	24 (4)	0.43 (20)	$10^+\rightarrow 8^+$
807.8 (9)	18 (4)		$(12^+)\rightarrow 10^+$
813.3 (4)	12 (5)		$(13^-)\rightarrow (11^-)$
818.4 (7)	<5		$(14^+)\rightarrow (12^+)$
842.5 (4)	29 (3)	0.17 (17)	$14^+\rightarrow 12^+$
991.0 (3)	27 (3)	-0.47 (23)	$7^{(-)}\rightarrow 6^+$
1048.9 (7)	19 (3)	0.31 (28)	$16^+\rightarrow 14^+$
1133.0 (2)	12 (3)		$(18^+)\rightarrow 16^+$
1276.7 (10)	13 (3)	-0.72 (42)	$5^{(-)}\rightarrow 4^+$

[a]Intensities taken from the 433.9 keV coincidence spectrum.

^{108}Pd 8^+ state at 2397.5 keV was found. The anisotropy and coincidence relationships of the depopulating 626.3 keV γ ray indicate a stretched $E2$ transition feeding the 6^+ state. However, the intensities of the 626.3, 777.2, and 991.0 keV γ rays in the 433.9 keV gated spectrum sum to $(123\pm 11)\%$ of the 723.1 keV intensity. Furthermore, the ratio of intensities of the 626.3 keV and 777.2 keV transitions in coincidence with the 614.2 keV $4^+\rightarrow 2^+$ is 0.26 ± 0.06 compared to 0.42 ± 0.06 for the 433.9 keV gate. It is therefore possible that the 626.3 keV γ ray feeds the 6^+ state through intermediate, unobserved transitions, with some strength feeding the 2^+ state through a separate branch. No γ rays linking the tentative 8_1^+ state with the 8_2^+ or either 10^+ state were observed. We place upper limits of less than 10% (2σ) of the 614.2 keV γ-ray intensity on such transitions.

Strongly populated negative-parity bands with band head spins of $(5–9)\hbar$ are a common feature of neutron-rich even-even palladium and cadmium nuclides. These typically feed into the ground band via strong ≈ 1 MeV $7^-\rightarrow 6^+$ and $5^-\rightarrow 4^+$ γ rays. A structure with similar properties has been identified in ^{108}Pd. A cascade which includes two γ rays (518.4 and 682.2 keV) whose anisotropies are consistent with stretched $E2$ multipolarity feeds the 6^+ state via a 991.0 keV transition and the 4^+ state via a 437.4–1276.7 keV branch. The 991.0 and 1276.7 keV γ rays have large negative anisotropies as expected for pure dipole transitions. Interference from the 433.9 keV $2^+\rightarrow 0^+$ line prevented accurate determination of the 437.4 keV transition multipolarity; the $I=5$ assignment to the 2324.8 keV state is based on the 1276.7 keV transition anisotropy, which is inconsistent with a $\Delta I=2$ assignment at the 2σ level. (A $\Delta I=0$ assignment would imply a highly unlikely octupole 437.4 keV γ ray.)

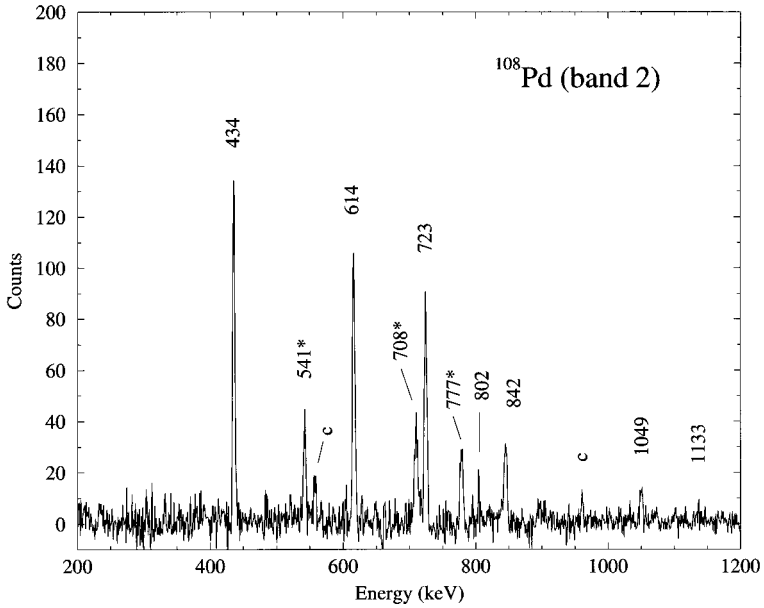

FIG. 4. The ground-state band of ^{108}Pd. Gating transitions are marked with asterisks and contaminant lines are marked ''*c*.''

The energy and spin of the 2324.8 keV state are consistent with a $\approx$2320 keV $L=5$ state seen in (t,p), (p,t), and (p,p') reactions [26].

In neighboring even-even nuclides, the analogous negative-parity bands are accompanied by similarly intense signature-partner bands, with $\Delta I=1$ transitions linking the bands near the bandheads. No evidence has been found in the present work for another negative-parity band in ^{108}Pd.

B. ^{107}Pd

The level scheme for ^{107}Pd deduced from the present work is shown in Fig. 5. Table II lists the energies, intensities, and anisotropies of γ rays assigned to this nuclide, along with deduced substate alignments, mixing ratios, and placements. Sample coincidence spectra for ^{107}Pd are shown in Fig. 6.

Band 1 in Fig. 5 is an yrast negative-parity band built on the isomeric 214.9 keV $11/2^-$ state. The band is extended from the previously known [27] $19/2^-$ state through the first angular-momentum alignment to $51/2\hbar$. For the higher transitions, the angular distributions are consistent with $E2$ multipolarity although the uncertainties are large. These uncertainties are indicated in Fig. 5 and Table II by parentheses on the level spins and parities.

Following completion of these analyses, results of an experiment in which ^{107}Pd was populated via the same reaction were published [7]. The level scheme of that work confirms the results for band 1 from the present work (first reported in Ref. [25]) up to the $39/2^-$ state, though with small discrepancies in transition energies.

At energies above 2 MeV, positive-parity states in ^{107}Pd are seen in three distinct bands, labeled 2, 3, and 4 in Fig. 5. Bands 2 and 3 appear to be signature-partner bands with strong $\Delta I=-1$ linking transitions, while band 4 is a decoupled $E2$ band. The bulk of the strength in the high-spin structures feeds into the negative-parity yrast band through $E1$ decays from the 19/2, 21/2, and 25/2 states, in a manner similar to that reported in ^{109}Cd [6,7]. The γ rays assigned to bands 2 and 3 above the $21/2^+$ state have also been reported in Ref. [7], although 704 keV and 1104 keV transitions shown in that work feeding the $33/2^+$ and $31/2^+$ states from a $35/2^+$ member of band 3 cannot be confirmed here due to interference from competing transitions.

Below 2 MeV, the band structure of the positive-parity states becomes less distinct. Bands 3 and 4 primarily feed into the $19/2^+$ state, which in turn decays by a decoupled $E2$ cascade to the 312.0 keV $7/2^+$ state. The ordering of states below the $17/2^+$ state is uncertain. While Fig. 5 represents the most likely ordering of the γ rays depopulating this state, the relative weakness of the transitions, combined with the difficulties due to multiple degenerate γ-ray pairs, allow the possibility that the ordering down to the $9/2^+$ state is reversed, i.e., the 677.7 and 644.2 lines may lie above the 772.6 and 805.8 transitions, with the 402, 404, and 368.2 keV lines placed appropriately. Evidence against this alternative includes the fact that the 392.5 keV line is significantly stronger than the 303.8 keV line in the 772.6 keV gate. If the order were reversed, the intensities would have to be equal. The intensity difference implies unseen branches from the 1374.0 keV $13/2^+$ state, though, which further indicates the uncertainty of the placements. (Interference from the 675.7 keV transition in band 4 prevents a similar comparison using a 677.7 keV gate.) The weakness of the 368.2, 402, and 404 keV lines precludes determination of the spin of the 1742.2 keV state. Values of 13/2, 15/2, and 17/2 are possible. The 677.7 and 772.6 keV transitions, as well as the 642.8, 721.5, and 696.9 keV γ rays of band 4 have also been reported by Juutinen *et al.* [7].

Klamra and Rekstad [27] first investigated high-spin states in ^{107}Pd using ^{104}Ru(α,n). They reported 643.3 and 808.5 keV transitions as the lowest members of a stretched $E2$ band built on a 312.8 keV $7/2^+$ state, based on weak coincidence data and detailed γ-ray angular distributions. More recently, Juutinen *et al.* [7] reported the low-lying members of band 4 with no mention of an 808 keV line. We have resolved the discrepancy by the discovery of the 805.8-644.2 keV cascade above the 696 keV $9/2^+$ state. This cascade weakly feeds the 312 keV state via the 384 keV line,

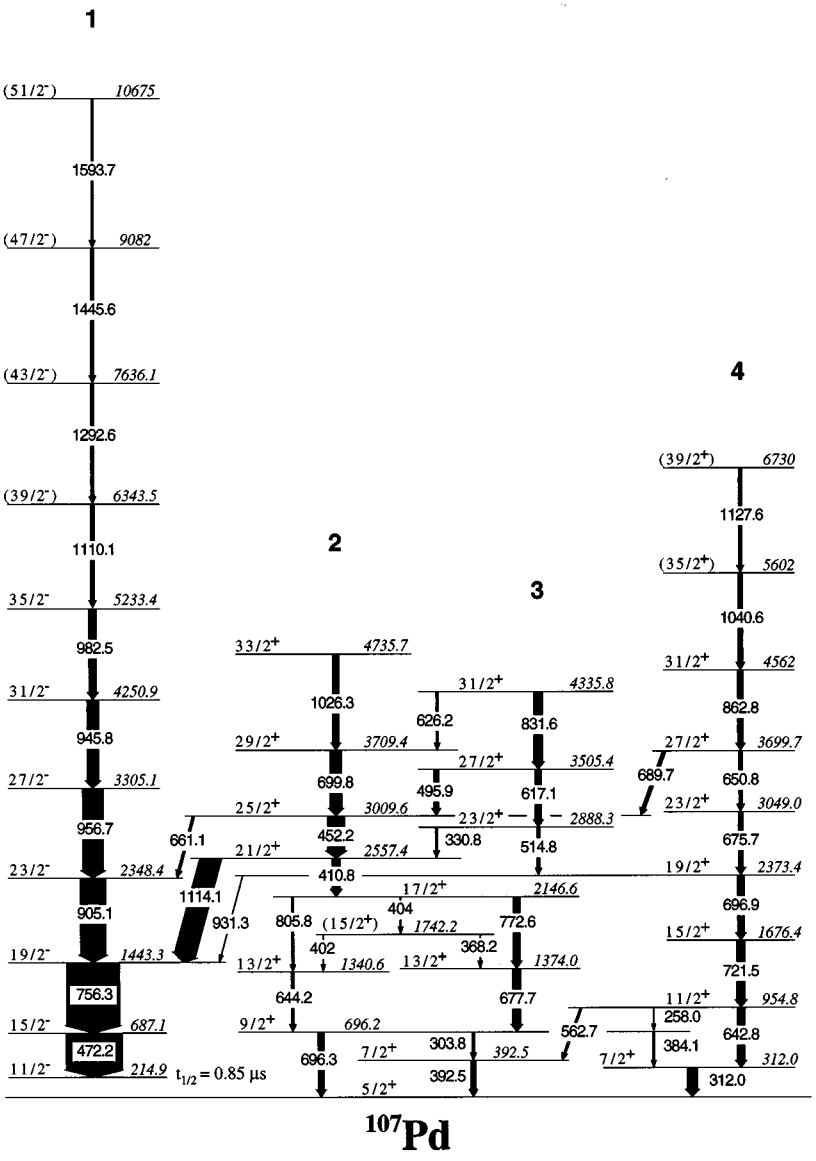

FIG. 5. Level scheme of ^{107}Pd.

explaining the coincidence relationships described in Ref. [27]. The 808.5 keV line in the spectrum shown in Ref. [27] appears to be unresolved from a lower-energy line. This may explain the 3 keV energy difference. No energy uncertainties are given in Ref. [27].

Other differences among the present work and the results of Refs. [27] and [7] are worth noting. First, although the anisotropy we report for the 312.0 keV line is consistent with the A_2 given in Ref. [27] (the anisotropy is approximately equal to A_2 for small values of A_4) we calculate an upper limit on the $E2/M1$ mixing ratio of -0.2 (using the phase convention of [28]) compared to their value of $-0.05^{+0.02}_{-0.03}$ (in the same phase convention); the difference is attributable to considerably different values of the substate alignment parameter: 0.5 ± 0.1 here versus ≈ 0.9 in that work. The value used in Ref. [27] was presumably chosen based on the apparent substate alignment of the feeding 643 keV line; the existence of the 644.2 line, which may have been stronger in the (α,n) reaction than the 642.8 line, may explain the relatively large substate alignment used. Also, while Ref. [7] reports substantially similar energies and anisotropies for the strongest γ rays in the positive-parity level scheme, most of the weaker lines in the present work, along with band 4, are new.

Finally, it is necessary to discuss the ordering of the 303.8-392.5 keV pair depopulating the $9/2^+$ state. States at both 302.8 and 392.5 keV are known from ^{107}Rh β^- decay [29], with the former being assigned $I^\pi=(3/2,5/2)^+$ based on (d,p) [30] and (d,t) [31] data. Clearly, the 392.5 keV state is fed by the 562.7 keV γ ray from the $11/2^+$ member of band 4, but the possibility that the $9/2^+$ state decays to the 302.8 keV state by a 393.5 keV γ-ray rather than (or as well as) decaying to the 392.5 keV state must be addressed. If this were the case, the 393.5 keV line would have to be stretched $E2$ in nature (with a 5/2 spin assignment for the 302.8 keV state) and would therefore have a positive anisotropy. The decay of the 302.8 keV state would be $5/2\rightarrow5/2$, and would also be expected to have a positive anisotropy (see Fig. 2). In fact, both lines are seen to have negative anisotropies (when gated on transitions above the $9/2^+$ state so as to eliminate the feeding of the $7/2^+$ state through the 562.7 keV transition). Based on this and the measured energy of 303.8 ± 0.2 keV rather than 302.8 keV, we conclude that although a decay branch from the $9/2^+$ state through the 302.8 keV state is

TABLE II. Properties of γ rays placed in ^{107}Pd.

Energy (keV)	Relative intensity	Anisotropy	Substate alignment [a]	$\delta(E2/M1)$	$I_i^\pi \rightarrow I_f^\pi$
258.0 (3)	0.5 (1)	−0.91 (90)	(0.5)	$\delta<0.15$	$11/2^+ \rightarrow 9/2^+$
303.8 (2) [b]	4.0 (3) [c]	−0.56 (30)	(0.5)		$9/2^+ \rightarrow 7/2^+$
312.0 (1)	18.9 (3)	−0.51 (10)	(0.5)	$\delta<-0.2$	$7/2^+ \rightarrow 5/2^+$
330.8 (3)	4.0 (7) [c]	−0.28 (22)	(0.7)	−0.1 (2)	$23/2^+ \rightarrow 21/2^+$
368.2 (2)	1.6 (2)				$(15/2)^+ \rightarrow 13/2^+$
384.1 (1)	2.7 (6) [c]	−0.46 (18)	(0.5)	$\delta<-0.1$	$9/2^+ \rightarrow 7/2^+$
392.5 (1) [b]	8.8 (3)	−0.42 (17)	(0.5)		$7/2^+ \rightarrow 5/2^+$
403.4 [d]	3.1 (2)				
410.8 (1)	14.2 (3)	0.18 (9)	0.39 (19)		$21/2^+ \rightarrow 17/2^+$
452.2 (1)	30.1 (3)	0.26 (7)	0.59 (15)		$25/2^+ \rightarrow 21/2^+$
472.2 (1)	100.0 (6)	0.23 (5)	0.47 (10)		$15/2^- \rightarrow 11/2^-$
495.9 (1)	9.5 (3)	0.16 (17)	(0.8)	0.30(15)	$27/2^+ \rightarrow 25/2^+$
514.8 (2)	5.2 (8) [c]	0.54 (40)			$23/2^+ \rightarrow 19/2^+$
562.7 (5)	4.0 (2) [c]	0.85 (30)			$11/2^+ \rightarrow 7/2^+$
617.1 (1)	11.8 (8)	0.25 (17)			$27/2^+ \rightarrow 23/2^+$
626.2 (2)	4.4 (5)	0.62 (27)	(0.9)	$0.45<\delta<1.9$	$31/2^+ \rightarrow 29/2^+$
642.8 (2)	14.4 (9) [c]	0.35 (11)	0.68 (21)		$11/2^+ \rightarrow 7/2^+$
644.2 (3)	5.5 (13) [c]				$13/2^+ \rightarrow 9/2^+$
650.8 (3)	6.4 (8)	0.59 (26)			$27/2^+ \rightarrow 23/2^+$
661.1 (4)	4.3 (6)	−0.37 (33)	(0.7)	$-0.15^{+0.25}_{-0.35}$	$25/2^+ \rightarrow 23/2^-$
675.7 (3)	8.3 (14) [c]	0.33 (15)			$23/2^+ \rightarrow 19/2^+$
677.7 (2)	14.7 (16) [c]	0.39 (15)	0.79 (30)		$13/2^+ \rightarrow 9/2^+$
689.7 (7)	6.4 (23) [c]	−0.37 (34)	(0.8)	−0.13 (26)	$27/2^+ \rightarrow 25/2^+$
696.3 (4)	11.3 (30) [c]	0.23 (23)			$9/2^+ \rightarrow 5/2^+$
696.9 (2)	12.0 (20) [c]	0.35 (19)			$19/2^+ \rightarrow 15/2^+$
699.8 (1)	20.8 (41) [c]	0.39 (14)	0.92 (33)		$29/2^+ \rightarrow 25/2^+$
721.5 (1)	15.1 (10) [c]	0.29 (13)	0.60 (27)		$15/2^+ \rightarrow 11/2^+$
756.3 (1)	93.7 (6)	0.24 (5)	0.53 (11)		$19/2^- \rightarrow 15/2^-$
772.6 (3)	12.2 (17)	0.16 (12)	0.34 (26)		$17/2^+ \rightarrow 13/2^+$
805.8 (7)	3.3 (10) [c]				$17/2^+ \rightarrow 13/2^+$
831.6 (4)	15.5 (40) [c]	0.20 (18)			$31/2^+ \rightarrow 27/2^+$
862.8 (1)	10.8 (4)	0.37 (19)			$31/2^+ \rightarrow 27/2^+$
905.1 (1)	45.4 (6)	0.31 (7)	0.71 (16)		$23/2^- \rightarrow 19/2^-$
931.3 (8)	1.0 (7)				$19/2^+ \rightarrow 19/2^-$
945.8 (1)	21.1 (8)	0.41 (13)	0.97 (32)		$31/2^- \rightarrow 27/2^-$
956.7 (1)	37.5 (8)	0.40 (10)	0.92 (24)		$27/2^- \rightarrow 23/2^-$
982.5 (2)	14.0 (15) [c]	0.24 (15)	0.58 (36)		$35/2^- \rightarrow 31/2^-$
1026.3 (1)	11.3 (4)	0.33 (15)			$33/2^+ \rightarrow 29/2^+$
1040.6 (2)	8.8 (4)	0.07 (21)			$(35/2^+) \rightarrow 31/2^+$
1110.1 (3)	7.2 (15) [c]	0.13 (22)			$(39/2^-) \rightarrow 35/2^-$
1114.1 (1)	38.3 (14)	−0.23 (13)	(0.7)	−0.05 (11)	$21/2^+ \rightarrow 19/2^-$
1127.6 (6)	6.1 (18) [c]	0.89 (45)			$(39/2^+) \rightarrow (35/2^+)$
1292.6 (3)	6.0 (5)	0.07 (23)			$(43/2^-) \rightarrow (39/2^-)$
1445.6 (3)	5.8 (6)	0.18 (27)			$(47/2^-) \rightarrow (43/2^-)$
1593.7 (3)	4.5 (22) [c]				$(51/2^-) \rightarrow (47/2^-)$

[a] Values in parentheses were determined from fit to quoted $E2$ substate alignments. Relative uncertainties in fitted substate alignments were taken to be 20%.

[b] The 303.8−392.5 keV coincident pair may be contaminated with a competing 302.8−393.5 keV pair. See text for details.

[c] Intensity taken from coincidence data.

[d] Unresolved doublet. The average energy and summed intensity of the γ rays are quoted.

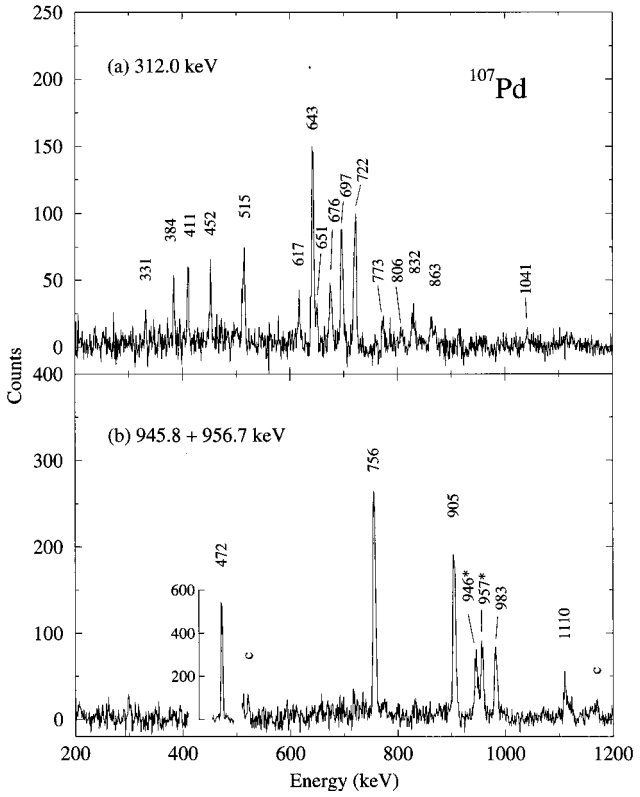

FIG. 6. Sample ^{107}Pd coincidence spectra. (a) Gate on 312.0 keV line (band 4). Note that some band 2 and band 3 transitions are present due to the linking 384.1 keV γ ray. (b) Sum of spectra gated on 945.8 and 956.7 keV lines (band 1). Contaminant lines are marked ''c.''

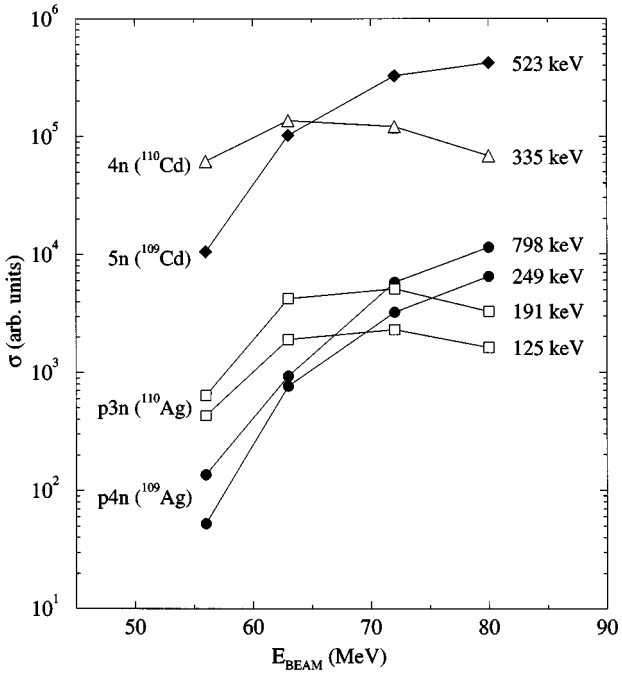

FIG. 7. Excitation functions for γ rays from the Penn ^{18}O + ^{96}Zr experiment. The 798 keV and 249 keV transitions placed in ^{109}Ag are shown with filled circles. 125 keV and 191 keV lines identified in ^{110}Ag are shown with open squares. 523 keV (filled diamonds) and 335 keV (open triangles) lines in ^{109,110}Cd, respectively, are shown for comparison. The cross sections are corrected for proton and γ-ray efficiencies.

possible, it is considerably weaker than the cascade through the 392.5 keV state shown in Fig. 5. (Since the 677.7 and 772.6 keV transitions were used to determine this, the arguments concerning their ordering are unchanged.) Interestingly, the opposite ordering (a 393 keV line feeding a 303 keV line) was found in the (α,n) reaction; in that case, the initial state was probably a known $1/2^+$ state near 697 keV. No lines were reported by Ref. [7] at either of these energies.

C. ^{109}Ag

Past work on ^{109}Ag has largely been limited to Coulomb-excitation [32], radioactive decay (cf. [33]), and direct reaction (cf. [34]) studies. These techniques, though, are ineffective tools for populating yrast states, which in other odd-A Ag isotopes are built on low-lying $g_{9/2}$ isomers. Consequently, although the corresponding isomers ($7/2^+$ at 88 keV and $9/2^+$ at 133 keV) have been seen in ^{109}Ag, no higher-spin states have been identified.

The strongest proton-evaporation channels from the ^{114}Cd compound nucleus were $p4n$ and $p3n$, leading to ^{109,110}Ag, respectively. Since no high-spin states were known in either nuclide, proton-gated excitation functions (shown in Fig. 7) from the Penn particle-γ experiment were used to identify candidate γ rays for each. (Note the factor of 50 difference in cross sections between the xn and pxn channels.) Coincidence relationships and gated angular distributions from the Chalk River p-γ-γ data were used to identify and place other lines in the ^{109}Ag level scheme, which is shown in Fig. 8. Measured intensities (from γ-γ coincidence data) and anisotropies for ^{109}Ag transitions are listed in Table III, along with deduced substate alignments, mixing ratios, and placements. Spectra gated on the 298.8 keV line (band 1) and 213.5 keV line (bands 2 and 3) are shown in Fig. 9. The experimental results for ^{110}Ag will be the subject of a future publication.

The low detection efficiency [due to absorption in the CsI(Tl) particle detectors] and high internal conversion probability for the known 44.7 keV $9/2^+ \rightarrow 7/2^+$ decay [35] prevented its detection in the Chalk River experiment, making it unclear whether the 798.0 and 640.6 keV transistions feed the $9/2^+$ or $7/2^+$ state. To resolve this and thereby firmly determine the yrast level scheme of ^{109}Ag, an additional experiment was performed to look for the 798.0-44.7 keV coincidence. In order to reduce interference from light Ag isotopes, the alternate reaction ^{100}Mo(^{13}C,$p3n$)^{109}Ag was chosen, which made use of the much higher isotopic enrichment of the ^{100}Mo target. The high resolution of the LEPS detector together with the lack of competing transitions near 45 keV obviated the need for channel selection.

Singles and 798.0 keV Ge-gated LEPS spectra are shown in Fig. 10. It is clear that the 798.0 keV line occurs in coincidence with the $\approx$ 44.7 keV $9/2^+ \rightarrow 7/2^+$ decay. Since a thin target was used, a correction for Doppler shift was made in determining the energy of this transition. Since the LEPS detector was centered at $\theta = 90°$, the correction would normally be quite small. However, the displacement of the re-

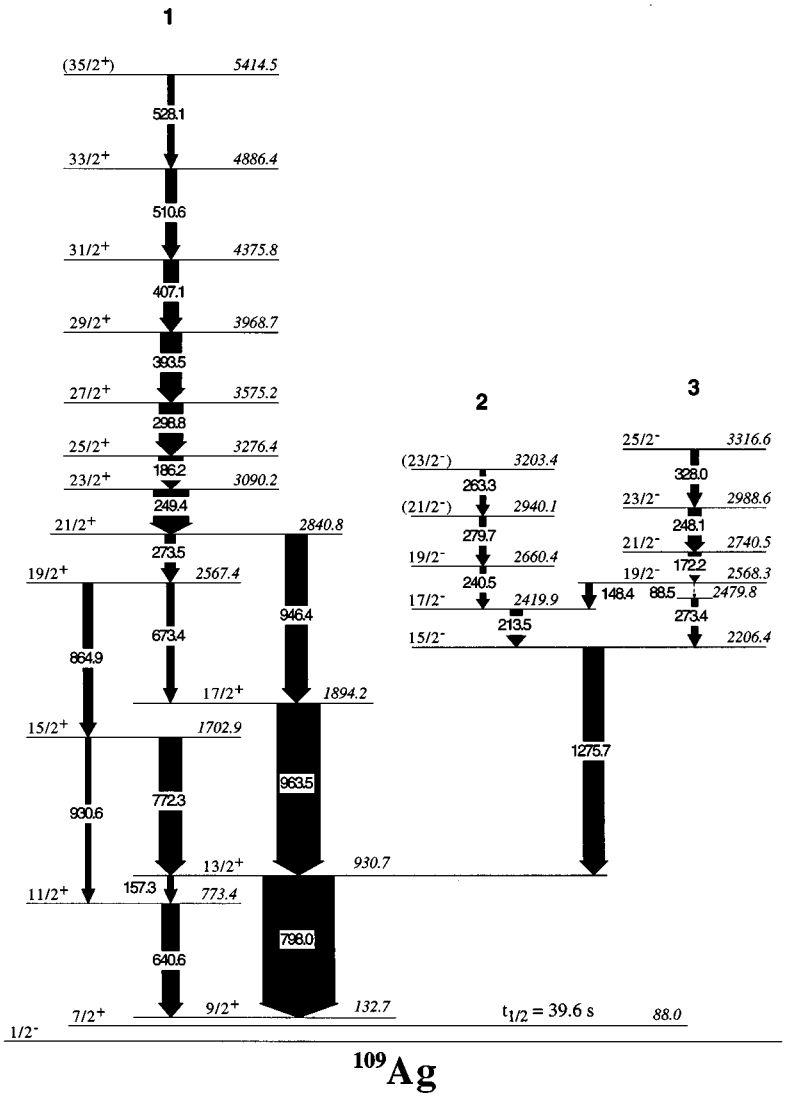

FIG. 8. Level scheme of ^{109}Ag.

coiling nucleus during (and prior to) the 2.6 ns isomeric decay is substantial ($v_{\text{recoil}} \times t_{1/2} \approx 0.8$ cm). After correcting for the Doppler shift, a fit to the LEPS singles spectrum gives an energy of 44.8 ± 0.1 keV for the decay, compared to an adopted value of 44.7 ± 0.2 keV [36].

The measured 798.0-44.8 keV coincidence intensity is a sensitive function of the $E2/M1$ mixing ratio of the 44.8 keV decay, since the internal conversion coefficients for $E2$ and $M1$ radiation at this energy are 26 and 4.3, respectively. Unfortunately, this sensitivity is somewhat washed out by angular correlation effects in the geometry chosen, especially when the recoil displacement is considered. A fit to the coincidence intensity assuming a $13/2 \rightarrow 9/2 \rightarrow 7/2$ decay pattern and an initial substate alignment of 0.45 yields a mixing ratio of $|\delta_{E2/M1}| = 0.35 \pm 0.15$. This is in very good agreement with an estimate of 0.30 ± 0.12 based on intensity balance arguments which use ^{109}Pd β^- decay data [36].

The resulting ^{109}Ag high-spin level scheme is qualitatively quite similar to those of the lighter silver isotopes ^{105,107}Ag [10,11]. At low energies, the dominant features are the two positive-parity signature-partner bands built on the $9/2^+$ isomer. The moderate signature splitting for these bands gives way to a strongly coupled $\Delta I = 1$ band (labeled band 1 in Fig. 7) above $21/2\hbar$ as with ^{105,107}Ag. Unlike the lighter isotopes, no $E2$ crossover transitions were seen above this state in ^{109}Ag. This is probably due to low statistics; lower limits on the $B(M1)/B(E2)$ ratios for band 1 above $21/2\hbar$ are generally consistent with the corresponding transition-strength ratios found in ^{105,107}Ag.

Two strongly coupled negative-parity bands were also seen. Again, while no $E2$ crossovers were found, the lower limits on the $B(M1)/B(E2)$ ratios are consistent with the ratios reported for the negative-parity bands in ^{105,107}Ag [10,11]. The ordering of bands 2 and 3 in Fig. 7 is based on intensities in coincidence with the 213.5 and 1275.7 keV lines, while the intensities listed in Table III are from a gate on the 798 keV line. Band 3 decays into the $15/2^-$ state through a 273.4 keV γ ray. However, the energy and intensity of the $\approx$88 keV linking transition could not be determined due to the high γ-ray attenuation at low energies in the particle-detector array, and it is possible that the 273.4 keV transition depopulates the $19/2^-$ state rather than feeding the $15/2^-$ state as shown in Fig. 8. Several of the lowest states in these bands (2206.4, 2568.3, and 2660.4 keV, as well as the 2567.5 keV $19/2^+$ state) are consistent with states

TABLE III. Properties of γ rays placed in ^{109}Ag.

Energy (keV)	Relative intensity	Anisotropy	Substate alignment [a]	$\delta(E2/M1)$	$I_i^\pi \rightarrow I_f^\pi$
44.8 (1)				± 0.35 (15)	$9/2^+ \rightarrow 7/2^+$
148.4 (1)	9 (1)	-0.16 (19)	(0.90)	$+0.05$ (11)	$19/2^- \rightarrow 17/2^-$
157.3 (1)	8 (1)				$13/2^+ \rightarrow 11/2^+$
172.2 (1)	18 (3) [b]	-0.23 (14)	(0.95)	$+0.01$ (8)	$21/2^- \rightarrow 19/2^-$
186.2 (1)	34 (1)	-0.31 (10)	(0.95)	-0.05 (5)	$25/2^+ \rightarrow 23/2^+$
213.5 (1)	17 (2) [b]	-0.36 (12)	(0.85)	-0.09 (8)	$17/2^- \rightarrow 15/2^-$
240.5 (2)	8 (2) [b]	-0.31 (16)	(0.90)	-0.05 (9)	$19/2^- \rightarrow 17/2^-$
248.1 (1)	18 (4) [b]	-0.20 (12)	(0.95)	$+0.02$ (8)	$23/2^- \rightarrow 21/2^-$
249.4 (1)	49 (5) [b]	-0.16 (7)	(0.95)	$+0.05$ (4)	$23/2^+ \rightarrow 21/2^+$
263.3 (2)	8 (3) [b]	-0.46 (16)	(0.95)	-0.14 (9)	$(23/2^-) \rightarrow (21/2^-)$
273.4 (3)	9 (3) [b]				$(17/2^-) \rightarrow 15/2^-$
273.5 (1)	15 (2) [b]	-0.18 (13)	(0.92)	$+0.03$ (8)	$21/2^+ \rightarrow 19/2^+$
279.7 (2)	9 (2) [b]	-0.02 (15)	(0.95)	$+0.13$ (9)	$(21/2^-) \rightarrow 19/2^-$
298.8 (1)	33 (1)	-0.35 (9)	(0.95)	-0.07 (5)	$27/2^+ \rightarrow 25/2^+$
328.0 (1)	11 (3) [b]	-0.13 (13)	(0.95)	$+0.06$ (8)	$25/2^- \rightarrow 23/2^-$
393.5 (1)	29 (1)	-0.13 (10)	(0.95)	$+0.06$ (4)	$29/2^+ \rightarrow 27/2^+$
407.1 (1)	21 (2) [b]	-0.22 (11)	(0.95)	0.00 (6)	$31/2^+ \rightarrow 29/2^+$
510.6 (2)	15 (2) [b]	-0.46 (15)	(0.95)	-0.14 (8)	$33/2^+ \rightarrow 31/2^+$
528.1 (3)	11 (2) [b]	0.10 (19)	(0.95)	$+0.20$ (14)	$(35/2^+) \rightarrow 33/2^+$
640.6 (2)	24 (1)	0.30 (9)	(0.50)	$+0.3 < \delta$	$11/2^+ \rightarrow 9/2^+$
673.4 (2)	12 (3) [b]	0.20 (19)	(0.85)	$+0.31$ (20)	$19/2^+ \rightarrow 17/2^+$
772.3 (3)	32 (5) [b]	0.50 (21)	(0.70)	$+1.0^{+1.0}_{-0.5}$	$15/2^+ \rightarrow 13/2^+$
798.0 (1)	100 (1)	0.22 (6)	0.44 (13)		$13/2^+ \rightarrow 9/2^+$
864.9 (4)	13 (4) [b]	0.61 (29)			$19/2^+ \rightarrow 15/2^+$
930.6 (8)	8 (3) [b]				$15/2^+ \rightarrow 11/2^+$
946.4 (1)	35 (1)	0.34 (11)	0.76 (24)		$21/2^+ \rightarrow 17/2^+$
963.5 (1)	60 (1)	0.43 (9)	0.90 (17)		$17/2^+ \rightarrow 13/2^+$
1275.7 (2)	29 (1)	-0.21 (12)	(0.90)	$+0.02$ (8) [c]	$15/2^- \rightarrow 13/2^+$

[a] Values in parentheses were determined from fit to quoted $E2$ substate alignments. Uncertainties were taken to range from ± 0.1 (at $\alpha = 0.5$) to ± 0.05 (at $\alpha = 0.95$).

[b] Intensity taken from coincidence data.

[c] Assigned as $E1$.

reported in ^{107}Ag(t,p) [34], although the precision of the direct-reaction measurements was only about 10 keV.

IV. DISCUSSION AND MODEL COMPARISONS

Although the nuclides in this mass region are known to have low-energy states which are vibrational in nature, the deformed rotor formalism has proven extremely successful in predicting their high-spin behavior. In particular, cranked shell model (CSM) calculations with BCS pairing [37] have been found to provide useful interpretations of the collective bands and band crossings of these nuclides. The nuclides studied here are predicted by total Routhian surface (TRS) calculations [38] to have somewhat larger and more stable deformations than the cadmium and light palladium isotopes previously interpreted with the CSM model ($\beta \approx +0.17$ compared to 0.10–0.15 for $^{106-110}$Cd and $^{104-106}$Pd) and should provide good tests for CSM predictions.

For all three nuclides, the adapted g reference described by Bengtsson *et al.* [37] based on the ^{108}Pd s band was used to choose the Harris reference parameters $\mathcal{J}_0 = 6\hbar^2/$ MeV and $\mathcal{J}_1 = 20\hbar^4/$ MeV^3. Pairing strength energies were chosen based on experimental odd-even mass differences. At zero frequency, strengths of $\Delta_\pi = 1.2$ MeV and $\Delta_\nu = 1.5$ MeV were used, with both decreasing to 50% of these values by $\hbar\omega = 0.8$ MeV.

TRS calculations for the vacuum configuration in ^{108}Pd are shown in Fig. 11. For rotational frequencies below 0.7 MeV, the energy surfaces show a prolate minimum at $\beta_2 =$ 0.17–0.21 and $\gamma \approx -5°$. (The static quadrupole moment of the ^{108}Pd 2^+ state is -0.58 e b [26], corresponding to a prolate rotor with $\beta_2 = 0.17$.) Similar minima are calculated for likely configurations of ^{107}Pd and ^{109}Ag, with $\beta_2 \approx 0.17$. Accordingly, deformations of 0.18 were chosen for use in CSM calculations for all three nuclides. The extreme γ softness of these minima suggests some freedom in choosing the triaxiality parameter in the CSM calculations, and axial symmetry ($\gamma = 0°$) was generally used. The hexadecapole parameter β_4 was set to zero for all calculations.

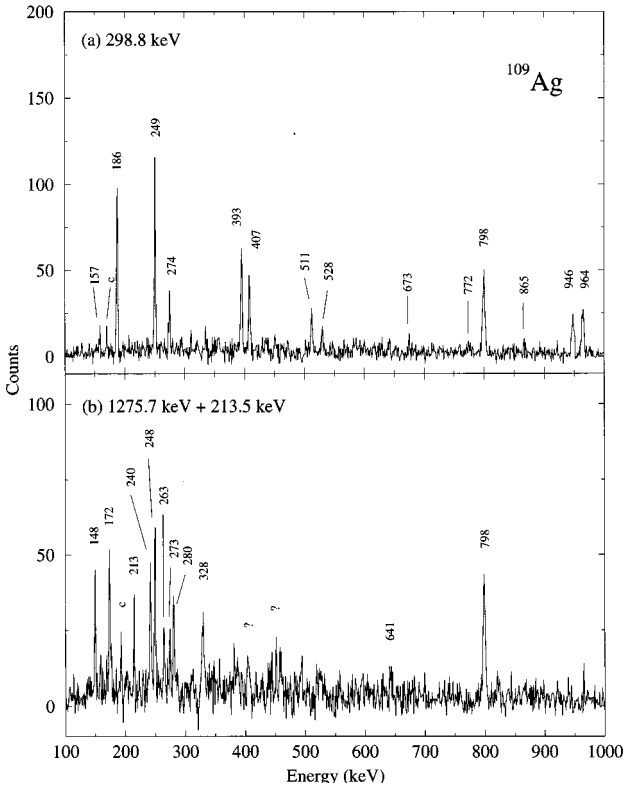

FIG. 9. Sample coincidence spectra in ^{109}Ag. (a) Gate on the 298.8 keV line in band 1. (b) Sum of spectra gated on the 1275.7 keV and 213.5 keV lines. A ''*c*'' indicates a contaminant line while a ''?'' indicates an unplaced ^{109}Ag transition.

Calculated quasiparticle Routhians for ^{108}Pd using these parameters are shown in Fig. 12. There are no significant differences between the Routhians for ^{108}Pd and those calculated for ^{107}Pd and ^{109}Ag. A list of the active neutron and proton orbitals is given in Table IV.

A. ^{108}Pd

The low-lying states of ^{108}Pd behave much like ''classic'' vibrational states. For instance, an $I=0,2,4$ triplet lies at about 1 MeV, 2.3 times the 2_1^+ energy, and the $B(E2;\ 4\rightarrow 2)$ and $B(E2;\ 2'\rightarrow 2)$ are almost twice the $B(E2;\ 2\rightarrow 0)$ [26]. Although lifetimes are not available for higher states, it is clear from the level spacings that this near-vibrational trend continues through the 8^+ state. Above the 8^+ state, though, the ground band is crossed by a band with rotational energy spacings, while the original ''vibrational'' sequence appears to continue up to spins of 14^+ as the non-yrast band 1.

A plot of the aligned angular momentum (i_x) for the two positive-parity bands is shown in Fig. 13. The first band crossing occurs at a frequency of $\hbar\omega\approx 0.33$ MeV and the yrast band gains almost $10\hbar$ of aligned angular momentum through the crossing. By comparison, the predicted quasineutron Routhian indicates a configuration change at about the same frequency due to the neutron $h_{11/2}^2$ (AB) crossing, with an increase of $9.2\hbar$ in i_x. The shape-polarizing property of the low-K $h_{11/2}$ pair is expected to stabilize the prolate minimum; this is indicated in the TRS calculation by a much deeper minimum along the β axis above the crossing frequency (see Fig. 11). By contrast, TRS calculations for the AB configuration above the first crossing (not shown) predict prolate first minima which are very soft along both the β and γ axes. This two-quasineutron configuration corresponds to the continuation of the ground-state configuration above the first crossing. The softness of the predicted minimum indicates continued vibrational behavior for the extension of the ground-state collective band above the crossing and reinforces the interpretation of band 1 as a vibrational structure.

The aligned angular momentum of the yrast band in the isotone ^{110}Cd is also shown in Fig. 13 for comparison. Note that while the ^{110}Cd *s* band crosses the ground-state band at

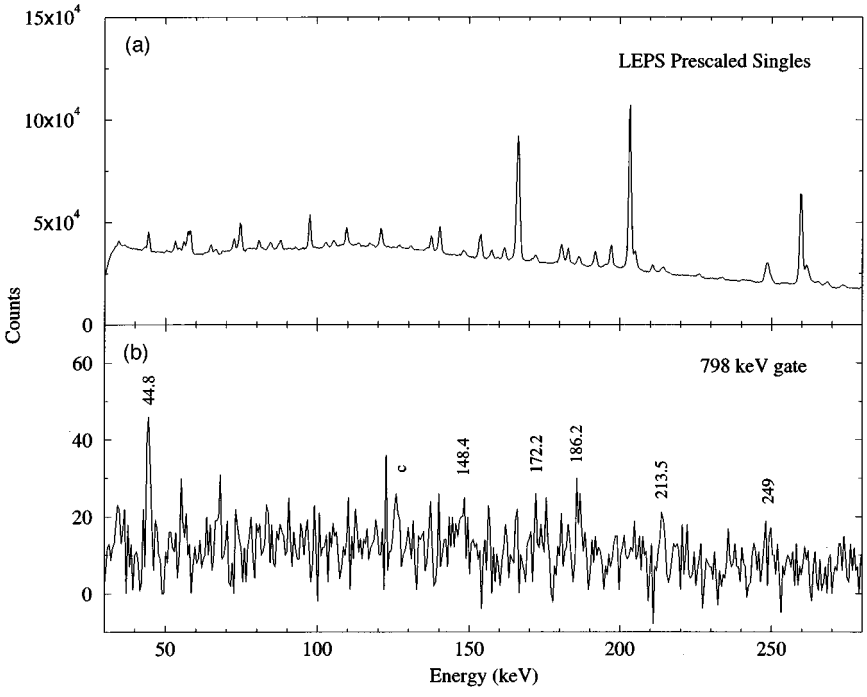

FIG. 10. LEPS spectra from the ^{13}C + ^{100}Mo experiment. (a) Singles downscaled by 10. (b) Gate on 798.0 keV in the Ge detector.

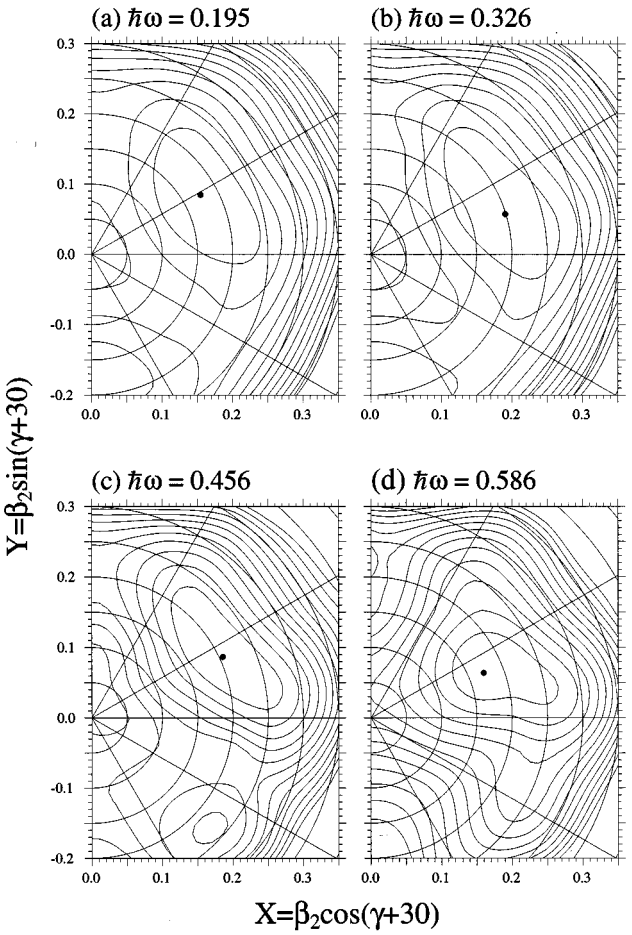

FIG. 11. TRS calculations for the ^{108}Pd vacuum. Contour lines are in 250 keV increments. (a) $\hbar\omega=0.195$ MeV: Minimum at $\beta_2=0.176$, $\gamma=-1°$, $E'=-1.35$ MeV with $I_x=1.1\hbar$; second minimum at $\beta_2=0.17$, $\gamma=-120°$, $E'=-1.26$ MeV. (b) $\hbar\omega=0.326$ MeV: Minimum at $\beta_2=0.199$, $\gamma=-13°$, $E'=-1.56$ MeV with $I_x=2.9\hbar$. The second minimum now has $E'=-1.22$. (c) $\hbar\omega=0.456$ MeV: Minimum at $\beta_2=0.205$, $\gamma=-5°$, $E'=-3.2$ MeV with $I_x=13.2\hbar$. (d) $\hbar\omega=0.586$ MeV: Minimum at $\beta_2=0.172$, $\gamma=-8°$, $E'=5.55$ MeV with $I_x=20.6\hbar$.

nearly the same frequency and exhibits the same amount of alignment, the interaction strength $|V_I|$ is about twice as strong in ^{108}Pd as in ^{110}Cd. CSM calculations for the two nuclides fail to predict this difference. Juutinen *et al.* [8] have suggested that the weak interaction in ^{110}Cd may be due to a shape difference between the two bands; the Routhian minimum is predicted to shift from $\beta_2=0.12$ to 0.17 through the crossing. This hypothesis is supported by the ^{108}Pd results, for which the TRS calculations predict a much smaller deformation change. An extension of the ^{110}Cd ground-state band above the first crossing is also shown in Fig. 13. It feeds into the yrast band at the 8^+ state, as with ^{108}Pd, and is in turn fed by a quasirotational band (band 17 of Ref. [8]) above the 14^+ state. Lifetime measurements of the 10^+ and 12^+ states of this sequence indicate fast collective transitions with $B(E2)>30$ W.u. [39] and the authors of Refs. [8] and [39] conclude that it is the vibrational continuation of the ground band above the crossing. The striking similarity between it and band 1 in ^{108}Pd supports a vibrational picture in ^{108}Pd as well.

The last point in the i_x plot for band 2 shows the beginning of another upbend near $\hbar\omega=0.55$ MeV. This could be the alignment of the second (CD) intruder neutron pair or the positive-parity EF neutron pair, both of which are predicted at around 0.65 MeV. However, in ^{110}Cd, where these neutron crossings should also occur near 0.65 MeV, two upbends are in fact seen close to the predicted frequencies. It therefore seems more likely that the observed upbend in ^{108}Pd at 0.55 MeV is due to the alignment of the proton $\frac{7}{2}^+$ [413] (ab) pair, predicted to occur near 0.48 MeV. It is important to remember that the predicted crossing frequencies are sensitive functions of the pairing gap parameters. The neutron strength $\Delta_\nu(\omega)$ is constrained by the observed AB crossing in ^{108}Pd and in turn restricts the CD crossing to a narrow range of freqencies. The proton strength $\Delta_\pi(\omega)$, though, is constrained only at $\omega=0$ by the odd-even mass difference; reasonable adjustments in the proton pairing strength parameters can delay the predicted ab crossing to above 0.5 MeV.

Negative-parity single-particle states in ^{108}Pd are likely to arise from neutron $h_{11/2}\otimes g_{7/2}^{-1}$, neutron $h_{11/2}\otimes d_{5/2}^{-1}$, proton $g_{9/2}\otimes p_{1/2}^{-1}$, and proton $g_{9/2}\otimes p_{3/2}^{-1}$ particle-hole states. These configurations have maximally aligned spins of 8^- and 9^- for the neutron states and 5^- and 6^- for the proton states, respectively. In this picture, the 5^- and 7^- states of band 3 would most likely be proton one-particle one-hole states. These negative-parity proton excitations should be largely insensitive to changes in neutron number, while the neutron excitations should drop in energy with increasing N as the neutron Fermi level approaches the $h_{11/2}$ shell. In fact, 5^- states do appear at nearly constant energies in $^{102-108}$Pd, but the 7_1^- states drop by more than 400 keV over the range. Also, as pointed out by Grau *et al.*, [13] the branching ratio $B(E2;\ 7^-\rightarrow5^-)/B(E1;\ 7^-\rightarrow6^+)$ drops by a factor of 33 from ^{104}Pd to ^{106}Pd. (The ^{108}Pd branching ratio is similar to the ^{106}Pd result.) Lifetime measurements of negative-parity bands in ^{110}Cd [39] indicate that the $\nu h_{11/2}\otimes\nu d_{5/2}^{-1}$ structures are built on nonmaximally aligned bandheads, which has led to speculation that they are semidecoupled configurations with the $d_{5/2}$ quasineutron deformation aligned. A similar situation may be occurring in ^{108}Pd, with the 7^- state forming the bandhead of a semidecoupled two-quasineutron band.

B. ^{107}Pd

As with other odd-N nuclides in this region, the yrast level scheme of ^{107}Pd is dominated by a decoupled rotational band built on a low-lying $\nu h_{11/2}$ isomer. The aligned angular momentum of this band (band 1) in ^{107}Pd is shown in Fig. 14. In contrast to the ^{108}Pd yrast band, no crossing is seen near $\hbar\omega=0.33$. Instead, the first alignment in ^{107}Pd is delayed, occuring at $\hbar\omega\approx0.48$ MeV. This is in good agreement with the CSM prediction, in which the odd quasineutron blocks the AB crossing, with the first crossing (BC) occurring at 0.45 MeV. The experimental alignment gain through the crossing is about $6.5\hbar$, also in good agreement with the predicted BC alignment gain of $6.3\hbar$. The quasiproton ab crossing is also predicted near 0.48 MeV, though with an increase of i_x of only $4.7\hbar$. While the observed crossing occurs closer to the predicted proton configuration change, the alignment gain is more consistent with

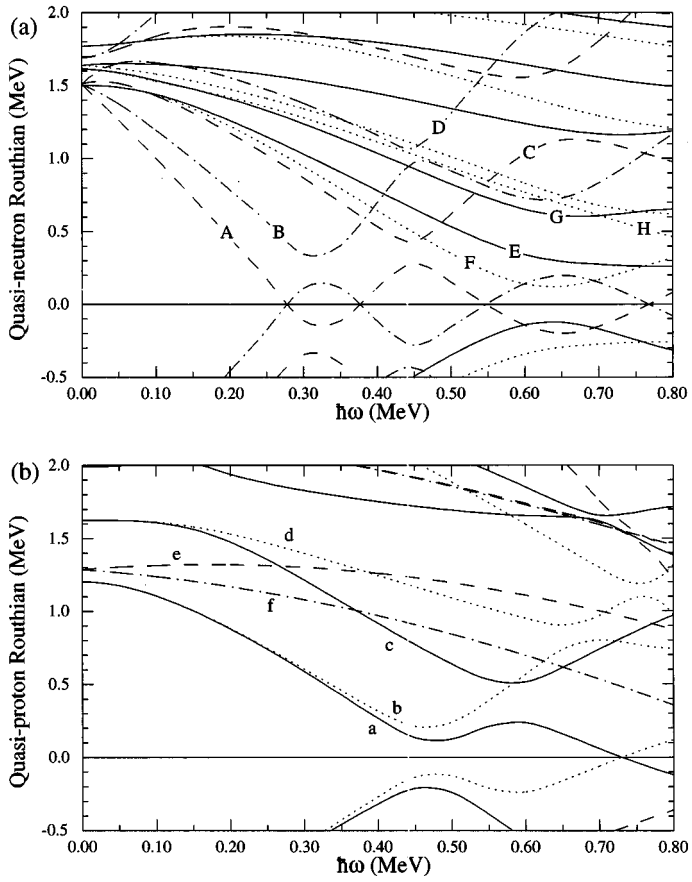

FIG. 12. Quasiparticle Routhians for (a) neutrons and (b) protons in ^{108}Pd. Calculations are for $\beta_2=0.18$, $\beta_4=0$, and $\gamma=0°$. Pairing strengths of $\Delta_\nu=1.5$ MeV and $\Delta_\pi=1.2$ MeV were used at zero frequency, falling by 50% at $\hbar\omega=0.8$ MeV. See Table IV for a list of the Routhian labels.

the predicted neutron alignment. The quasiproton alignment should occur at the same rotational frequency in both ^{107}Pd and ^{108}Pd, since the crossing frequency is reasonably insensitive to the predicted difference in deformations. The second upbend in the ^{108}Pd yrast band (at $\hbar\omega\approx0.55$ MeV) is interpreted as being caused by the proton ab crossing, so one would expect a similar crossing frequency for the ^{107}Pd alignment. This implies that the ^{107}Pd alignment at 0.48 MeV is quasineutron in nature, with the three-quasineutron $\nu(h_{11/2})^3$ ABC configuration above the crossing.

This assignment is corroborated by the crossing frequencies of the neighboring odd-N nuclides ^{105}Pd and ^{109}Cd. Due to its smaller deformation, the BC crossing in ^{109}Cd is predicted to occur later than the BC crossing in ^{107}Pd. In ^{105}Pd, the corresponding crossing should occur at an even higher frequency since, in addition to the reduced deformation, the neutron $h_{11/2}$ orbitals lie further from the Fermi level. In fact, the measured crossings occur near 0.51 MeV in ^{109}Cd [6] and 0.56 MeV in ^{105}Pd [40], as expected.

TABLE IV. Active orbitals for $\beta_2\approx0.17$.

Particle	CSM label $\alpha=-1/2$	CSM label $\alpha=+1/2$	Dominant configuration Spherical	Dominant configuration Nilsson	g factor [a]
Neutrons	A	B	$h_{11/2}$	$1/2^-$ [550]	-0.21
	C	D	$h_{11/2}$	$3/2^-$ [541]	-0.21
	F	E	$g_{7/2}$	$5/2^+$ [413] [b]	$+0.21$
	H	G	$d_{5/2}$	$3/2^+$ [411] [b]	-0.33
Protons	b	a	$g_{9/2}$	$7/2^+$ [413]	$+1.27$
	d	c	$g_{9/2}$	$5/2^+$ [422]	$+1.27$
	e	f	$p_{1/2}$	$1/2^-$ [310]	-0.23

[a]From Lönnroth *et al.* [44].

[b]At $\beta_2=0.17$, these states contain significant components other than the asymptotic orbital listed.

Interpretation of the low-lying positive-parity states in the context of the cranked shell model is difficult. The dominant configurations are predicted to be the Nilsson $\frac{3}{2}^+$ [411] and $\frac{5}{2}^+$ [413] orbitals of $d_{5/2}$ and $g_{7/2}$ parentage. The $5/2^+$ ground state of ^{107}Pd has been assigned $L=2$ and the 312.0 keV $7/2^+$ state $L=4$ from direct reaction data [30,31]. At deformations of $\beta_2\lesssim0.2$ these Nilsson basis states are strongly mixed, and the predicted quasineutron states are further mixed when the nucleus is ''cranked.'' A strong interaction is predicted near $\hbar\omega=0.15$ MeV, with the predominantly $g_{7/2}$ Routhian dropping below the $d_{5/2}$. The picture is further complicated by the fact that the low-spin core excitations are vibrational, not rotational, in nature. In light of these difficulties, comparison of the low-energy states with rotational-model predictions does not seem fruitful at this time. (We note that similar states in lighter odd-A Pd nuclides have been interpreted in the context of a particle-core coupling model with much success [40–42]. These comparisons, however, rely heavily on detailed measurements of non-yrast states, which are typically not populated in heavy-ion fusion-evaporation reactions.)

The theoretical interpretation of the high-energy states is clearer. The cranked shell model predicts that the bands built

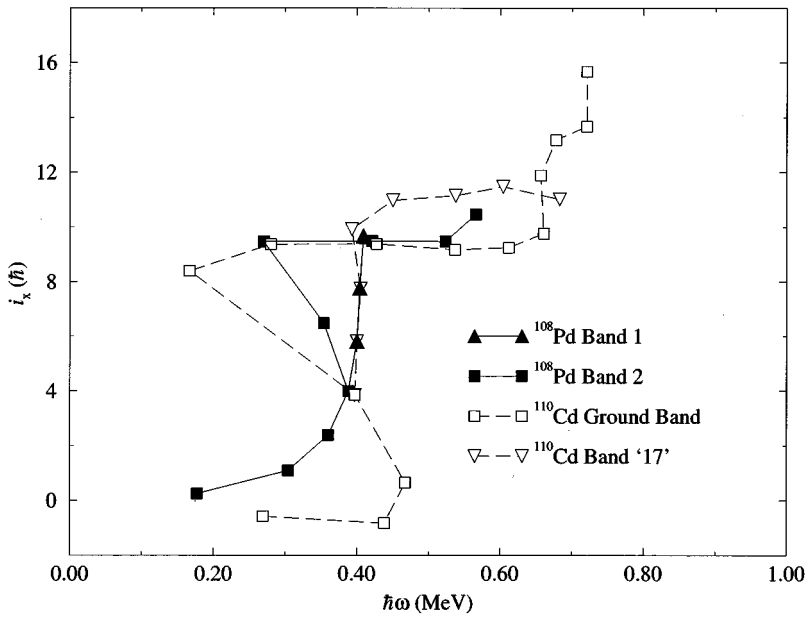

FIG. 13. Aligned angular momentum i_x for positive-parity bands in ^{108}Pd and ^{110}Cd. Closed symbols are for ^{108}Pd and open symbols are for ^{110}Cd. Squares indicate the yrast band while triangles indicate the ground band above the first alignment.

on both positive-parity configurations should undergo back bends near $\hbar\omega = 0.3$ MeV due to the alignment of the AB quasineutron pair. Since this rotational alignment is seen in both ^{106}Pd [13] and ^{108}Pd, one expects the $L \approx 6-10$ collective excitations of the ^{107}Pd core to be sufficiently rotational for the alignment to be seen here as well. Indeed, the ^{107}Pd positive-parity bands undergo alignments at rotational frequencies of 0.25–0.33 MeV, as shown in Fig. 14. (For completeness, the 642.8, 721.5, and 696.9 keV lines are used in both the band 3 and band 4 plots, and band 2 is assumed to proceed through the 772.6 and 677.7 keV γ rays in the order shown in Fig. 5. $K = 5/2$ was used for all three bands.) The ^{108}Pd ground band is also shown for comparison.

Three important features of these plots should be noted. First, all three bands gain at least $8\hbar$ of aligned angular momentum through the crossing. This gain in i_x is in good agreement with the CSM prediction for the quasineutron AB crossing, and is larger than the alignment gain predicted for any other crossing. Second, the ^{107}Pd positive parity bands align at lower frequencies than the ^{108}Pd ground band (or the ^{106}Pd ground band, which aligns near 0.36 MeV [13]). Again, this is in good agreement with the predicted AB crossing. The unpaired neutron in ^{107}Pd is expected to reduce the pairing strength, which in turn allows the alignment to proceed at lower frequencies. Finally, all three bands appear to be undergoing the alignment as they begin. This feature is hard to interpret with the CSM model. One possible explanation is that since the CSM predicts the bands should interact strongly at low frequencies, the first few data points are perturbed. A more likely explanation is that the initial ''upbending'' is caused by a vibrational energy spacing.

Experimental Routhians for bands 1–4 are shown in Fig. 15. K values and level orderings were chosen in the same manner as for Fig. 14. Above the alignment, the $M1$ transitions linking bands 2 and 3 clearly indicate these bands con-

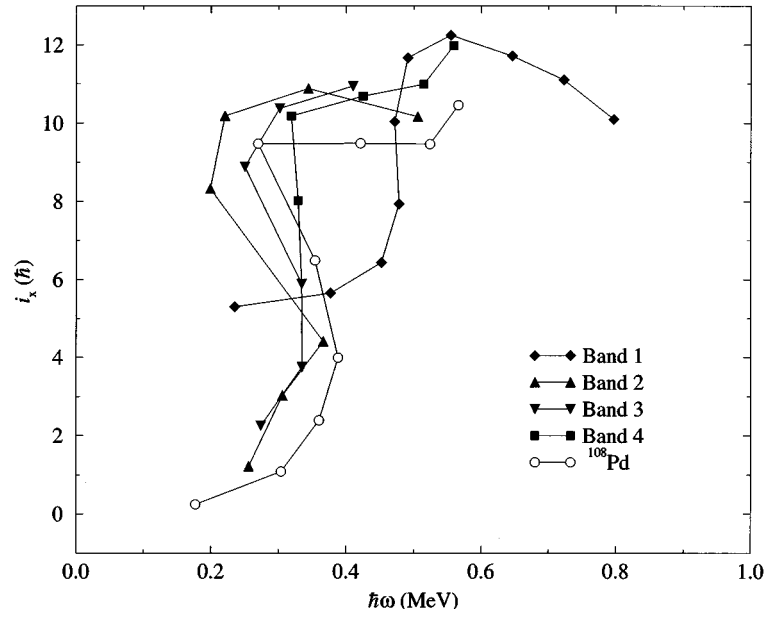

FIG. 14. Aligned angular momentum i_x for ^{107}Pd bands. $K = 1/2$ was used for band 1 (diamonds); $K = 5/2$ was used for bands 2 and 3 (triangles) and band 4 (squares). The yrast $7/2^+$, $11/2^+$, and $15/2^+$ states were included in the plots for both bands 3 and 4. Band 2 of ^{108}Pd is shown for comparison.

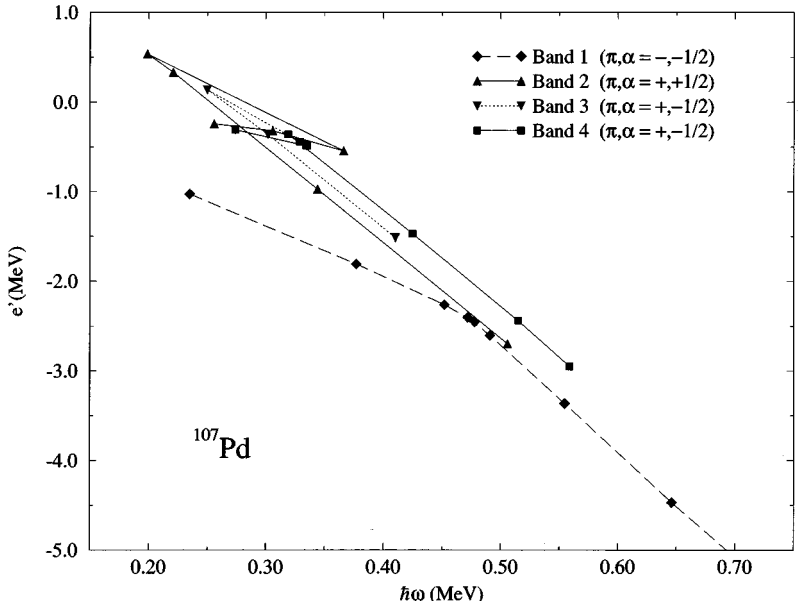

FIG. 15. Experimental Routhians for ^{107}Pd bands. The parameters were the same as for Fig. 14. The yrast $7/2^+$, $11/2^+$, and $15/2^+$ states were included in the plots for both bands 3 and 4.

stitute signature partners with band 2 favored. The signature splitting $\Delta e'$ is 0.2 MeV, with the favored signature α_f equal to $+1/2$, suggesting these bands are $d_{5/2}$ in nature. Band 4, with $\alpha=-1/2$, lies about 0.4 MeV above band 2. No candidate signature partner for band 4 was found. Since the usual assumption for heavy-ion fusion-evaporation reactions is that states closer to the yrast line are preferentially populated over states farther away, we conclude that the signature partner to band 4 is raised in energy by the signature splitting, and band 4 is favored.

These results are in disagreement with the axially symmetric CSM calculations, in which the $\alpha=-1/2$ signature of the lowest positive-parity quasineutron Routhian pair (E-F) lies about 200 keV *lower* than the $\alpha=+1/2$ signature. The next pair (G-H) lies about 500 keV higher and has the $\alpha=+1/2$ signature lower than the $\alpha=-1/2$. If bands 2 and 3 correspond to the EAB and FAB configurations, and band 4 to HAB, then the experimental signature partners are ''inverted'' for both the E-F and G-H Routhians. On the other hand, if bands 2 and 3 are identified as GAB and HAB, the CSM incorrectly places the G and H Routhians $\approx$400 keV above the E and F states, rather than 400 keV below.

The failure of axially symmetric CSM calculations to predict the observed structure is not surprising. The ^{107}Pd results reported here are quite similar to published results for the corresponding three-quasineutron bands in ^{109}Cd [6,7], indicating this behavior is a general property of the $N=61$ nuclides below the proton shell gap and is relatively insensitive to changes in the deformation or proton number. In Ref. [6], we interpreted the corresponding signature inversion in ^{109}Cd as an indication of γ softness or triaxiality. TRS predictions for the two nuclides suggest that these configurations should be even more γ soft for ^{107}Pd.

The TRS surfaces shown in Fig. 11 predict minima at $\gamma\approx-5°$. Although CSM calculations for ^{107}Pd with $\gamma<0°$ fail to reproduce the observed ordering, calculations with $\gamma\approx+20°$ do show signature inversions for both the EF and GH pairs at $\hbar\omega\lesssim0.45$ MeV, in good agreement with the observed results. Note, however, that TRS calculations for these configurations in ^{107}Pd do not predict a triaxial minimum, but rather a γ-soft prolate minimum, as stated previously. The agreement between the observed signature ordering and the triaxial CSM calculation may, therefore, be coincidental.

To further investigate the nature of these bands, one may turn to the transition strengths and mixing ratios. The semiclassical geometrical model [28] of Dönau and Frauendorf gives predictions for the $B(M1;\ I\rightarrow I-1)/B(E2;\ I\rightarrow I-2)$ ratios and the $E2/M1$ mixing ratio. In an extension of this model published by Radford *et al.*, [43]

$$B(M1;I\rightarrow I-1)=\frac{3}{8\pi I^2}\left\{\sqrt{I^2-K^2}\left[\left(1\pm\frac{\Delta e'}{\hbar\omega}\right)\tilde{g}_1K_1+\tilde{g}_2K_2+\tilde{g}_3K_3+\cdots\right]-K[\tilde{g}_1i_1+\tilde{g}_2i_2+\tilde{g}_3i_3+\cdots]\right\}^2\mu_N^2 \quad (2)$$

where

$$\tilde{g}_i=g_i-g_R \quad (3)$$

and

$$K=K_1+K_2+K_3+\cdots. \quad (4)$$

Subscript 1 indicates the quasiparticle responsible for the observed signature pair while other subscripts refer to ''spectator'' quasiparticles. The plus sign in the signature-splitting term should be used for favored-to-unfavored transitions, and the minus for unfavored-to-favored. A rigid rotor estimate for the $B(E2)$ strength is used to predict the $B(M1)/B(E2)$ ratio. In this model, the sign of the $E2/M1$ mixing ratio for the $I\rightarrow I-1$ transition is

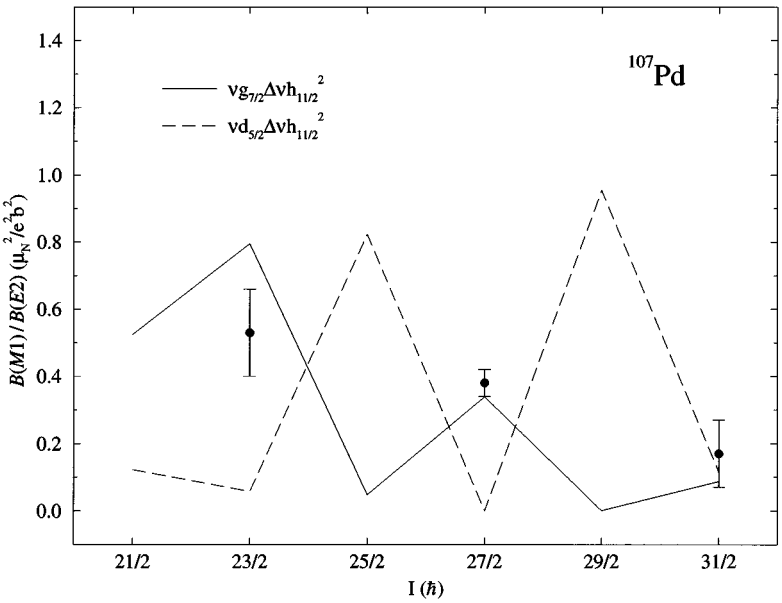

FIG. 16. Transition strengths for ^{107}Pd band 3 decays. Experimental $B(M1)/B(E2)$ ratios are shown as points. Geometrical model predictions assuming $\nu g_{7/2}\otimes\nu(h_{11/2})^2$ (solid line) and $\nu d_{5/2}\otimes\nu(h_{11/2})^2$ (dashed line) configurations are shown for comparison.

$$\mathrm{sgn}(\delta_{E2/M1}) = \mathrm{sgn}(Q_0)\times\mathrm{sgn}\Bigg(\sqrt{I^2-K^2}\Bigg[\left(1\pm\frac{\Delta e'}{\hbar\omega}\right)\tilde{g}_1K_1 + \tilde{g}_2K_2+\tilde{g}_3K_3+\cdots\Bigg] - K[\tilde{g}_1i_1+\tilde{g}_2i_2+\tilde{g}_3i_3+\cdots]\Bigg) \quad (5)$$

where Q_0 is positive for prolate shape. For the calculations described here, an intrinsic quadrupole moment of $Q_0=+2.1\ e$ b, corresponding to $\beta_2\approx 0.17$, was used and the collective factor g_R was set to Z/A. Gyromagnetic factors g_i for the active states (taken from Ref. [44]) are listed in Table IV, and K was assumed to equal Ω for each orbital.

Experimental $B(M1)/B(E2)$ ratios for the high-spin states of band 3 are plotted in Fig. 16. Also shown are the geometrical model predictions for bands 2 and 3 assuming $\nu g_{7/2}\otimes\nu(h_{11/2})^2$ (quasiparticle labels EAB and FAB) and $\nu d_{5/2}\otimes\nu(h_{11/2})^2$ configurations (GAB and HAB). The data appear to be more consistent with the $g_{7/2}$ prediction. This is reinforced by the $E2/M1$ mixing ratios for the $I\rightarrow I-1$ decays, which are positive for the $27/2^+$ and $31/2^+$ decays, and consistent (at 1σ) with a positive sign for the $23/2^+$ decay. The geometrical model predicts positive mixing ratios for $\nu g_{7/2}\otimes\nu(h_{11/2})^2$ and negative mixing ratios for $\nu d_{5/2}\otimes\nu(h_{11/2})^2$. We conclude that bands 2 and 3 are predominantly $\nu g_{7/2}\otimes\nu(h_{11/2})^2$ (EAB and FAB) above the $21/2^+$ state, with the signatures inverted (as compared to the axial CSM calculations). Band 4 is then presumably the $\alpha=-1/2$ signature of the $\nu d_{5/2}\otimes\nu(h_{11/2})^2$ configuration (HAB); again it appears likely that the experimental signatures for this configuration are inverted.

C. ^{109}Ag

The decay scheme of ^{109}Ag reported here is quite similar to the previously reported [10,11] schemes of ^{105,107}Ag. At low energies, the yrast cascades of all three nuclides (and ^{111}Ag [45]) are found to consist of positive-parity intermediate-coupled signature partners with moderate signature splitting. Popli *et al.* [46] have shown, using quasiparticle-plus-rotor calculations, that the ^{105,107}Ag bands are consistent with a $g_{9/2}$ quasiproton assignment, as expected for $Z=47$ at intermediate prolate deformations. Since the neutron number should influence these states only indirectly (through the core deformation) the similarity of these bands in the three nuclides suggests a similar configuration assignment for ^{109}Ag. The energies of these yrast bands in ^{105}Ag and ^{107}Ag are virtually identical [10,11]. In comparison, the ^{109}Ag level spacings are compressed by about 10% from the lighter isotopes, and the ^{111}Ag $13/2^+$-$9/2^+$ spacing is compressed by 20% [45], suggesting progressively larger core deformations as predicted by TRS calculations.

The theoretical quasiproton Routhians shown in Fig. 12(b) show the positive-parity positive-signature $\pi g_{9/2}$ Routhian a as energetically favored. The observed signature splitting of 0.2–0.3 MeV near $\hbar\omega=0.4$ MeV lies between the predicted ab splitting of ≈ 0.1 MeV and the predicted cd splitting of ≈ 0.4 MeV.

As with the lighter isotopes, both signatures of band 1 undergo large alignments near the $21/2^+$ state, as shown in Fig. 17. The crossing occurs near $\hbar\omega=0.33$ MeV, as expected for a neutron $(h_{11/2})^2$ alignment. The large gain in aligned angular momentum is also consistent with the predicted quasineutron alignment. Above the crossing, the signature splitting disappears. This is reasonably consistent with the aAB and bAB configurations, but not the cAB and dAB configurations, which are predicted to have a significant signature splitting for $\hbar\omega>0.2$ MeV.

In the one-quasiparticle-plus-rotor calculations of Popli *et al.* [46], the yrast bands of ^{105,107}Ag are predominantly $K\approx 7/2$–$9/2$ near the bandhead, with the Coriolis force mixing in progressively more low-K components as the core rotation increases. The experimentally determined $B(M1)/B(E2)$ ratios (including limits for unobserved transitions) both below and above the $\nu(h_{11/2})^2$ alignment are plotted in Fig. 18. Geometrical model predictions for $K_\pi=5/2$, $7/2$, and $9/2$ are also plotted. In all cases, the signature splitting

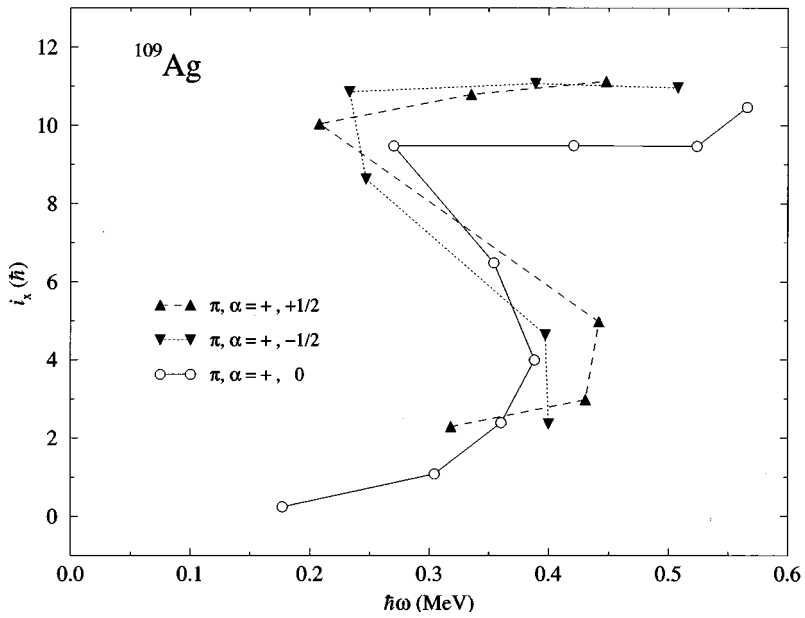

FIG. 17. Aligned angular momentum i_x for band 1 of ^{109}Ag (triangles), assuming $K=7/2$. Band 2 of ^{108}Pd (circles) is shown for comparison.

below the alignment induces very large oscillations (of order 10 to 1) in the predicted ratios which are absent in the experimental data. In order to compare the average magnitude of the transition-strength ratios, we have therefore arbitrarily set the signature splitting term in the model prediction to zero. Below the quasineutron alignment, the experimental ratios are less than 6 $\mu_N^2/(e\mathrm{b})^2$ and appear to decrease with increasing spin. This is consistent with the model predictions assuming $K=7/2$ or 5/2, especially given the prediction of Popli *et al.* that the contribution of the lower-K orbitals should increase with increasing spin. The $K=9/2$ prediction of large [$>15\mu_N^2/(e\mathrm{b})^2$] ratios is inconsistent with the experimental results. Above the alignment, the lower limits on the experimental ratios are consistent with the $K=9/2$ or 7/2 prediction, but not with the $K=5/2$ prediction.

Bands 2 and 3 are strongly coupled negative-parity bands whose Routhians lie about 1.5 MeV above that of the one-quasiproton positive-parity band. Bands with decay properties similar to band 2 have been reported in ^{105,107}Ag [10,11].

The lowest-lying theoretical negative-parity proton Routhians are the e-f pair originating from the $p_{1/2}$ orbital. These are predicted to lie about 0.5 MeV above the a and b Routhians, with a large (>0.2 MeV) signature splitting, small i_x, and weak $M1$ transitions. The experimentally observed bands are clearly inconsistent with all these properties and are therefore almost certainly three quasiparticle bands. The most likely configurations are one quasiproton (a or b) coupled to two quasineutrons (AE or AF), i.e., $\pi g_{9/2}\otimes\nu h_{11/2}\otimes\nu g_{7/2}$ or $\pi g_{9/2}\otimes\nu h_{11/2}\otimes\nu d_{5/2}$. These are predicted to lie 1–2 MeV above the one-quasiproton band with $i_x\approx 8$, in good agreement with the experimental results. Geometrical model $B(M1)/B(E2)$ ratios for these bands are very large at the spins observed, which is consistent with the nonobservation of crossover transitions. The possible observation of some of these states in ^{107}Ag(t,p) [34] is puzzling, and may be a coincidence. [The uncertainty in the (t,p) ex-

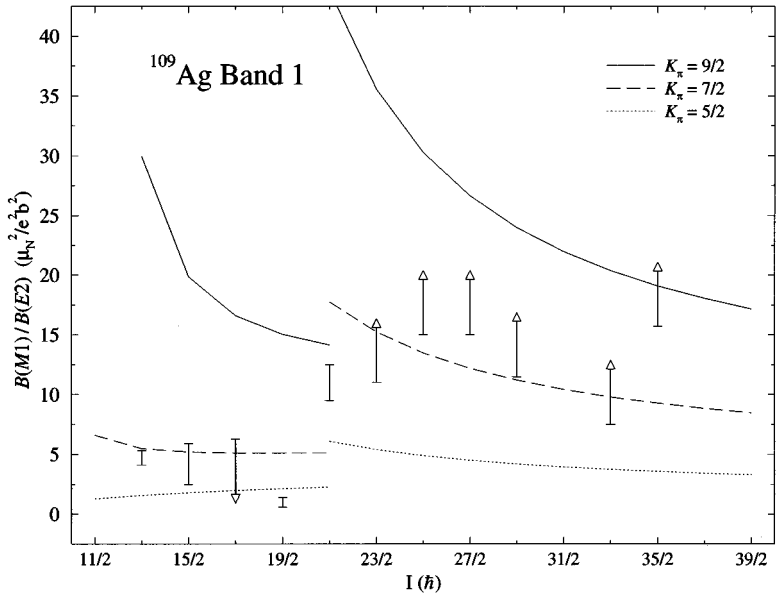

FIG. 18. Transition strengths for ^{109}Ag band 1 decays. Experimental $B(M1)/B(E2)$ ratios and 1σ limits are shown with error bars and arrows. Geometrical model predictions assuming $\pi g_{9/2}$ (below $I=21/2\hbar$) and $\pi g_{9/2}\otimes\nu(h_{11/2})^2$ (above $I=21/2\hbar$) are also shown for proton K values of 9/2 (solid lines), 7/2 (dashed lines), and 5/2 (dotted lines). The model calculations do not include the measured signature splittings, which induce very large fluctuations below $I=21/2\hbar$.

citation energies is approximately 10 keV.] If these states were observed in the transfer reaction, they would have to contain significant $\pi p_{1/2}\otimes(\nu)^2$ components, possibly eAB and fAB or eEF and fEF. These should lie much higher, though, and have large signature splittings. Another possibility is that these bands represent the three-quasiproton configurations abe and abf. These, however, should also exhibit a large signature splitting and weak $M1$ transitions.

V. SUMMARY AND CONCLUSIONS

High-spin states in ^{107,108}Pd and ^{109}Ag have been investigated using charged-particle-γ, γ-γ, and charged-particle-γ-γ coincidence methods. These measurements provide the first data on high-spin states in ^{109}Ag, while the yrast decay schemes of ^{107}Pd and ^{108}Pd have been substantially extended. The technique of charged-particle-γ-γ coincidence measurement is found to be particularly effective for selectively analyzing weak charged-particle evaporation channels in a neutron-rich fusion-evaporation reaction.

All three nuclides studied are found to have yrast collective bands with properties consistent with predictions for moderately deformed prolate rotors. While the detailed structures of each are different, all are found to be strongly influenced by the presence of the deformation-driving neutron $h_{11/2}$ low-K intruder orbitals.

In the even-even nuclide ^{108}Pd, the ground band has been extended to $I^\pi=18^+$, with new positive- and negative-parity sidebands observed to 14^+ and 13^-. The vibrational band built on the ground state is crossed by a rotational sequence near $I=8\hbar$. The crossing frequency and aligned angular momentum are similar to those of the corresponding band in the isotone ^{110}Cd, and are consistent with CSM and TRS predictions for a $\nu(h_{11/2})^2$ configuration at $\beta_2\approx 0.18, \gamma=0°$. Evidence is also seen for the beginning of a quasiproton alignment at higher frequencies. A positive-parity sideband extending above the 8^+ state appears to be the continuation of the vibrational ground band above the band crossing, while the negative-parity band may represent a semidecoupled configuration with both deformation-aligned and rotation-aligned quasineutrons.

The $\nu h_{11/2}$ band in ^{107}Pd has been extended through a band crossing to $51/2^-$. The band crossing seen in ^{108}Pd is not observed in this band, in good agreement with the quasineutron ''blocking'' predicted by the CSM model. An alignment seen at higher frequencies is interpreted as the predicted crossing with the $\nu(h_{11/2})^3$ band. Three positive-parity bands are also found at spins above $21/2\hbar$. These are interpreted as a decoupled $\nu d_{5/2}\otimes\nu(h_{11/2})^2$ band and both signatures of the $\nu g_{7/2}\otimes\nu(h_{11/2})^2$ configuration, based on $E2/M1$ mixing ratios and transition-strength ratios. For both configurations, the experimental signatures are inverted, possibly due to γ softness or triaxiality. Below the $21/2^+$ state, the positive-parity decay scheme lacks distinct rotational bands, possibly due to a relaxation to near-spherical vibrational modes. Such a transition would further highlight the ''core-polarizing'' role (seen in ^{108}Pd) of the $h_{11/2}$ intruder as a principal cause of the nuclear deformation.

The high-spin decay scheme of ^{109}Ag has been investigated for the first time. As with other odd-A Ag isotopes, at low energies the yrast structure is found to consist of intermediate-coupled signature partner bands produced by coupling collective core excitations to a high-K $g_{9/2}$ proton. This is crossed by a strongly coupled band with large i_x at the same rotational frequency as the ^{108}Pd crossing. The alignment gain, crossing frequency, and reduction in signature splitting are all consistent with a CSM prediction of a quasineutron $(h_{11/2})^2$ alignment. The increase in $B(M1)/B(E2)$ ratios through the crossing is also consistent with geometrical model calculations for a two-quasineutron alignment. Two strongly coupled negative-parity bands have also been identified. These may represent $\pi g_{9/2}\otimes\nu h_{11/2}\otimes\nu g_{7/2}$ or $\pi g_{9/2}\otimes\nu h_{11/2}\otimes\nu d_{5/2}$ configurations.

ACKNOWLEDGMENTS

We thank Dr. R. Wadsworth for loaning us the ^{96}Zr target used at Chalk River and Dr. R. Darlington for making the ^{96}Zr and ^{100}Mo targets used at the University of Pennsylvania. Thanks are also due Dr. D. Radford for providing the RADWARE data analysis software and Dr. R. A. Wyss for supplying the CSM and TRS codes. We appreciate the help given by J. Vasek and J. Middleton at the University of Pennsylvania, and G. Zwartz and J. L. Rodriguez in performing the experiment at Chalk River. We also thank Dr. D. Winchell for helpful discussions. This work was supported by the National Science Foundation, Atomic Energy of Canada Limited, and the Natural Sciences and Engineering Research Council (Canada).

[1] P. H. Regan *et al.*, J. Phys. G **19**, L157 (1993).
[2] D. Jerrestam *et al.*, Nucl. Phys. **A571**, 393 (1994).
[3] P. H. Regan *et al.*, Nucl. Phys. **A586**, 351 (1995).
[4] D. Jerrestam *et al.*, Nucl. Phys. **A545**, 835 (1992).
[5] I. Thorslund *et al.*, Nucl. Phys. **A568** 305 (1994).
[6] P. H. Regan *et al.* Phys. Rev. C **49**, 1885 (1994).
[7] S. Juutinen *et al.*, Nucl. Phys. **A577**, 727 (1994).
[8] S. Juutinen *et al.*, Nucl. Phys. **A573**, 306 (1994).
[9] P. H. Regan (private communication).
[10] D. Jerrestam, W. Klamra, J. Gizon, B. Fogelberg, S. J. Freeman, H. J. Jensen, S. Mitarai, G. Sletten, and I. Thorslund, Nucl. Phys. **A579**, 256 (1994).
[11] D. Jerrestam, W. Klamra, J. Gizon, F. Lidén, L. Hildingsson, J. Kownacki, Th. Lindblad, and J. Nyberg, Nucl. Phys. **A577**, 786 (1994).
[12] D. Jerrestam *et al.*, Nucl. Phys. **A557**, 411c (1993).
[13] J. A. Grau, L. E. Samuelson, F. A. Rickey, P. C. Simms, and G. J. Smith, Phys. Rev. C **14**, 2297 (1976).
[14] A. O. Macchiavelli, J. Burde, R. M. Diamond, C. W. Beausang, M. A. Deleplanque, R. J. McDonald, F. S. Stephens, and J. E. Draper, Phys. Rev. C **38**, 1088 (1988).
[15] R. Aryaeinejad *et al.*, Phys. Rev. C **48**, 566 (1993).
[16] J. A. Shannon *et al.*, Phys. Lett. B **336**, 136 (1994).
[17] S. K. Khosa and P. K. Mattu, Phys. Rev. C **38**, 1498 (1988).

[18] T. Chapuran, J. W. Arrison, D. P. Balamuth, and J. Görres, Nucl. Instrum. Methods Phys. Res. Sect. A **272**, 767 (1988).
[19] H. R. Andrews *et al.*, Internal Report No. AECL/8329, 1984.
[20] A. Galindo-Uribarri, Prog. Part. Nucl. Phys. **28**, 463 (1992).
[21] M. Behar, K. S. Krane, R. M. Steffen, and M. E. Bunker, Nucl. Phys. **A201**, 126 (1973).
[22] L. I. Gover, A. M. Demidov, I. B. Shukalov, M. R. Ahmed, K. I. Shakarchi, S. Al-Najjar, M. A. Al-Amili, and N. Al-Assafi, Nucl. Phys. **A245**, 13 (1975).
[23] I. Y. Lee, N. R. Johnson, F. K. McGowan, R. L. Robinson, M. W. Guidry, L. L. Riedinger, and S. W. Yates, Phys. Rev. C **25**, 1865 (1982).
[24] J. L. Durell, in *Proceedings of the International Conference on Spectroscopy of Heavy Nuclei, Crete, Greece, 1989*, edited by J. F. Sharpey-Schafer and L. D. Skouros (Institute of Physics, Philadelphia, 1990).
[25] K. R. Pohl *et al.*, Bull. Am. Phys. Soc. **38**, 1857 (1993).
[26] Jean Blachot, Nucl. Data Sheets **62**, 803 (1991).
[27] W. Klamra and J. Rekstad, Nucl. Phys. **A258**, 61 (1976).
[28] F. Dönau and S. Frauendorf, in *Proceedings of the Conference on High Angular Momentum Properties of Nuclei*, Oak Ridge, TN, 1982, edited by N. R. Johnson (Harwood, New York, 1983), p. 143.
[29] H. C. Griffin and W. R. Pierson, Phys. Rev. **183**, 991 (1969).
[30] B. L. Cohen, J. B. Moorehead, and R. A. Moyer, Phys. Rev. **161**, 1257 (1967).
[31] R. C. Diehl, B. L. Cohen, R. A. Moyer, and L. H. Goldman, Phys. Rev. C **1**, 2086 (1970).
[32] M. Loiselet, O. Naviliat-Cuncic, and J. Vervier, Nucl. Phys. **A496**, 559 (1989).
[33] W. C. Schick, Jr., and W. L. Talbert, Jr., Nucl. Phys. **A128**, 353 (1969).
[34] R. E. Anderson, J. J. Kraushaar, I. C. Oelrich, R. M. DelVecchio, R. A. Naumann, E. R. Flynn, and C. E. Moss, Phys. Rev. C **15**, 123 (1977).
[35] G. Berzins, M. E. Bunker, and J. W. Starner, Nucl. Phys. **A114**, 512 (1968).
[36] Jean Blachot, Nucl. Data Sheets **64**, 913 (1991).
[37] R. Bengtsson, S. Frauendorf, and F. R. May, At. Data Nucl Data Tables **35**, 16 (1986).
[38] R. Wyss, J. Nyberg, A. Johnson, R. Bengtsson, and W. Nazarewicz, Phys. Lett. B **215**, 211 (1988).
[39] M. Piiparinen *et al.*, Nucl. Phys. **A565**, 671 (1993).
[40] F. A. Rickey, J. A. Grau, L. E. Samuelson, and P. C. Simms, Phys. Rev. C **15**, 1530 (1977).
[41] Rakesh Popli, F. A. Rickey, and P. C. Simms, Phys. Rev. C **22**, 1121 (1980).
[42] J. A. Grau, F. A. Rickey, G. J. Smith, P. C. Simms, and J. R. Tesmer, Nucl. Phys. **A229**, 346 (1974).
[43] D. C. Radford *et al.*, Nucl. Phys. **A545**, 665 (1992).
[44] T. Lönnroth, S. Vajda, O. C. Kistner, and M. H. Rafailovich, Z. Phys. A **317**, 215 (1984).
[45] S. Zeghib, F. A. Rickey, G. S. Samuda, P. C. Simms, and Ning Wang, Phys. Rev. C **36**, 939 (1987).
[46] Rakesh Popli, J. A. Grau, S. I. Popik, L. E. Samuelson, F. A. Rickey, and P. C. Simms, Phys. Rev. C **20**, 1350 (1979).